[Frontiers in Bioscience 9, 309-337, January 1, 2004]

PROTON AND ELECTRON TRANSFER IN THE ACCEPTOR QUINONE COMPLEX OF PHOTOSYNTHETIC REACTION CENTERS FROM *RHODOBACTER SPHAEROIDES*

Colin A. Wraight

Department of Biochemistry and Center for Biophysics & Computational Biology, MC–147, University of Illinois, 607 South Mathews Avenue, Urbana, IL 61801, U.S.A.

TABLE OF CONTENTS

1. ABSTRACT

For twenty years the photosynthetic reaction center (RC) has been the premier testing ground for theoretical understanding of electron transfer in aperiodic systems, with special, but not unique, reference to long distance biological electron transport. In addition to the known structure, many of the attributes that make RCs so well suited to studying electron transfer function equally well for any charge movement, including protons. These include the presence of intrinsic reporter groups (electrochromically active pigments), high time resolution through light activation, and a large number and variety of distinct reactions, ranging from loosely coupled responses of the protein dielectric to specific, long distance proton transfers in and out of active sites, and bond making in terminal chemical transformations. A wide variety of biophysical methods have been coupled with site directed mutagenesis to reveal mechanisms of proton uptake, transfer and chemistry in the RC. This review summarizes our progress to date, which suggests that the RC can serve as a paradigm, not only for many energy coupled, membrane proteins, but for the electrostatic and dielectric properties of proteins that are critical to their general function.

2. INTRODUCTION

The function of all photosynthetic reaction centers is to convert light energy into metastable oxidizing and reducing equivalents, by charge separation, and to export these in a mobile form for subsequent utilization in "energy coupled" electron transport chains, ultimately driving ion transport and ATP synthesis (1-3). In reaction centers of purple bacteria and in Photosystem II of oxygenic organisms, reducing equivalents are exported in

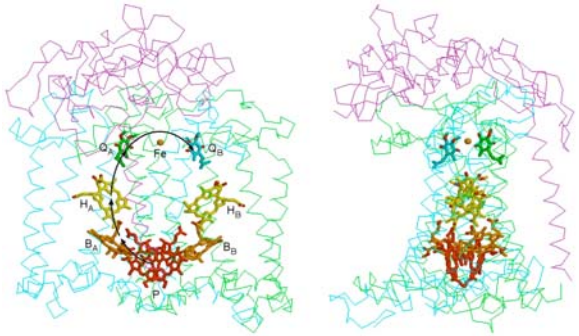

Figure 1. The photosynthetic reaction center from *Rhodobacter (Rba.) sphaeroides*. The L, M and H subunits are shown as backbone traces in green, blue and magenta, respectively. The two views shown are roughly orthogonal. The membrane plane runs from left to right, with the cytoplasmic phase at the top and the extracellular (periplasmic) space at the bottom. Note that the H-subunit significantly caps the structure over Q_A, while Q_B is much less protected. The polyisoprene groups of all cofactors have been truncated (Q_A and Q_B) or removed (chlorins). The active electron transfer path is indicated by arrows, in the left hand figure. The structure file used was 1aig.pdb.

pairs as reduced quinol, requiring coordinated uptake of protons (4). Of obvious importance in its own right, the elucidation of the structure of the bacterial reaction center, almost two decades ago (5, 6), motivated extraordinary progress in our knowledge of membrane proteins, generally, as well as leading to a sophisticated understanding of biological electron transfer (3, 7).

The properties of light activation, known structure and a plethora of intensely absorbing cofactors made the bacterial reaction center (RC) a powerful tool for studying electron transfer (ET). The same features make it a very effective model system for intraprotein proton transfer (PT). Although not alone here, the RC presents exceptional opportunities for studying diverse issues regarding proton uptake and proton transfer in protein functions, including:

1. charge compensation and conformational relaxation,
2. bond making/breaking in coupled ET/PT to or from hydrogen carriers,
3. coordination of proton delivery with electron transfer and substrate binding/release.

Net proton uptake by RCs is the result of quinol production, which requires 2H+ per $2e^-$ (4, 8). Indirect coupling of electron transfers to proton uptake is also seen in reponse to light-induced perturbation of the charge distribution of the protein. The important function of proton pumping, which is characteristic of cytochrome oxidase (9, 10) and bacteriorhodopsin (11), is not carried out by RCs but the main features of long distance H^+ transfer, essential to pumping mechanisms, are well represented in the pathway of proton delivery in the reaction center. This review will address proton transfer events coupled to the electron transfer reactions of quinone reduction in isolated reaction centers from *Rhodobacter (Rba.) sphaeroides* and *capsulatus,* with some reference to reaction center function in the native membrane system (chromatophores).

3. THE REACTION CENTER STRUCTURE

The functional core of the reaction center (RC) complex from purple photosynthetic bacteria is a heterodimer of similar, but non-identical, proteins (subunits L and M), plus a third polypeptide (subunit H) that caps the LM dimer on the cytosolic side of the membrane (Figure 1) (for review, see (12, 13)). The LM dimer binds all the cofactors, while subunit H stabilizes the structure and is involved in H^+-ion uptake and transfer associated with electron transfer to the quinones. The L and M subunits and all associated cofactors are arranged around a quasi-2-fold rotational symmetry axis, normal to the plane of the membrane and passing through the primary donor (P, a dimer of bacteriochlorophyll, Bchl) and a ferrous (Fe^{2+}) iron midway between the two quinones. Electron transfer proceeds from the excited singlet state of the primary donor (P*), *via* the monomer Bchl (B_A) to the bacteriopheophytin (H_A) bound to the L subunit. From H_A^-, the electron is transferred to the primary quinone, Q_A, which is bound in a fold of the M subunit, and from Q_A^- it crosses the symmetry axis to reach the secondary quinone, Q_B, bound in a similar fold of the L subunit. The sequence of events is (14-16):

$$P^* \xrightarrow{3\,ps} B_A \xrightarrow{1\,ps} H_A \xrightarrow{0.2\,ns} Q_A \xrightarrow{10\text{-}100\,\mu s} Q_B$$

The two quinones constitute a functional "acceptor quinone complex", organized around the central iron atom and its ligand field of four histidines and a glutamate (Figure 2). Q_A and Q_B are both bound with the C1 carbonyl hydrogen bonded to a backbone NH, and the C4 carbonyl hydrogen bonded to the $N_\delta H$ of a histidine ligand of the iron atom.

The early events of photosynthesis, from the excited state of the primary donor (P*) to the reduction of Q_A, involve cofactors that are tightly bound as "prosthetic groups". Q_B, on the other hand, is in weak binding equilibrium when fully oxidized or reduced. If it is present, Q_B is reduced by electron transfer (ET) from Q_A^- and becomes tightly bound as the semiquinone, Q_B^-. In the presence of a secondary donor, P^+ is rereduced and the RC can again be photoactivated, which provides a second electron, also *via* Q_A^-, to doubly reduce Q_B to the quinol state, QH_2 (hydroquinone), with the uptake of protons from the solution:

Scheme 1

1st flash:

$$Q_A Q_B \xrightarrow{h\nu} \underset{(H^+)_a}{Q_A^- Q_B} \longleftrightarrow \underset{(H^+)_b}{Q_A Q_B^-}$$

2nd flash:

$$\underset{(H^+)_b}{Q_A Q_B^-} \xrightarrow{h\nu} Q_A^- Q_B^- \longleftrightarrow Q_A^- Q_B H \longleftrightarrow Q_A Q_B H_2 \overset{\longleftarrow [2-b]H^+ \longrightarrow}{\rightleftharpoons} \underset{Q}{Q_A Q_B} \quad \underset{QH_2}{}$$

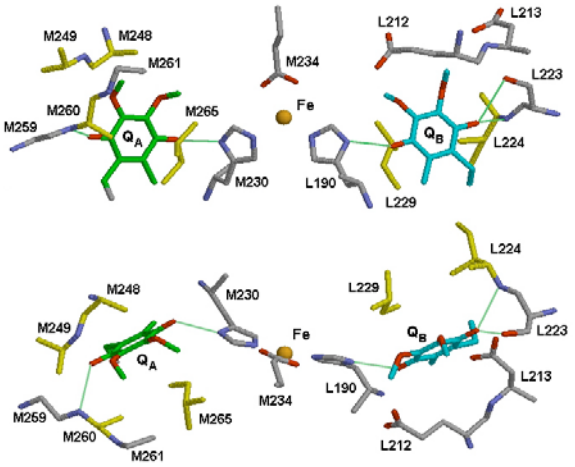

Figure 2. The acceptor quinone complex of the Rba. sphaeroides reaction center. QA (green) and QB (cyan) are bound around an iron-histidine ligand complex (two histidines, L230 and M266, are omitted). Top: view from the membrane plane (similar to Fig. 1, left). Bottom: view from the cytoplasmic surface (approximately 90° rotated from top panel view). The two quinone binding sites are similar and are related by the pseudo-2-fold rotational axis of the reaction center. QB is shown in its proximal position (see text). Not all contact residues are shown, but both sites are predominantly non- or weakly polar, except for GluL212 and AspL213 in the QB site. Hydrophobic residues are shown in yellow (AlaM248, AlaM249, AlaM260, IleM265, IleL224, IleL229). Each quinone is hydrogen bonded through its C4 carbonyl to a histidine (N□H) and through the C1 carbonyl to a backbone amide (NH). In the semiquinone anion form, QB is also hydrogen bonded by SerL223 (OH), as shown. The side chains of M259 (asparagine) and M261 (threonine) are omitted for clarity; they do not contact the quinone headgroup. Coordinates are from 1dv3.pdb.

The involvement of protons is crucial for both electron transfers to Q_B, with contributions that are energetic, kinetic and structural.

Following photoactivation, the first electron is shared between the two quinones. The negative charges of the anionic semiquinones induce proton uptake to the protein, contributing to the partial shielding and stabilization of the semiquinones (17-19). Full reduction of Q_B is coupled with the delivery of two protons to the quinone head group, to form QH_2, which leaves the RC and is replaced by an oxidized quinone from the membrane pool. This returns the acceptor quinones to their original state and allows RC turnover to proceed under multiple-flash activations. Under such conditions, binary oscillations can be seen in the formation and disappearance of semiquinone and in the uptake of protons from the medium (b<1 on the first flash, 2-b on the second, in Scheme 1) (for review, see (8, 20, 21)).

4. CHARGE COMPENSATION AND PROTEIN RELAXATIONS

Following light absorption, the appearance of separated charges inside the RC is a rude insult to its dark-adapted equilibrium state, and a process of microscopic adjustment begins immediately, to accommodate the *de novo* charges of P^+ and the sequentially reduced acceptors. These motions constitute the dielectric response of the protein, and occur over an enormous time range. Some responses are very rapid and precede and accompany the early electron transfers between the acceptors (22-24). However, significant relaxation also occurs following reaction, for example throughout the lifetime of the $P^+Q_A^-$ state, from the subnanosecond to millisecond range (25).

Changes in proton distribution within the protein can contribute to the compensation of the new charge states, but the time scale of the relaxations may not allow for a substantial contribution from net proton uptake. The total extent of relaxation in the $P^+Q_A^-$ state, alone, is on the order of 120 meV, but is 75% complete prior to 1 μs (25), whereas net H^+ uptake occurs much later than this (26). Thus, the H^+ binding can contribute no more than about 30 meV, and probably much less, to the total stabilization of this charge separated state. However, the dielectric capabilities of the protein reflect its internal structure and dynamics, which will include protons *already* bound to groups, and this changes with pH.

From basic principles, the integrated proton uptake associated with a reaction reflects the influence that protonation has on the energetics of the process, according to (19, 27):

$$2.303RT\int \Delta H^+ . dpH = \delta\Delta G \qquad \text{Eqn. 1}$$

ΔH^+ is the proton uptake associated with the formation of a particular state, e.g., $PQ_A \rightarrow PQ_A^-$, and $\delta\Delta G$ represents the pH-dependent contribution to the free energy of the reaction, relative to a reference pH at which the integration is started. This is of particular importance to the function of the acceptor quinones, because the free energy difference between the two charge states is small, and small differential contributions can dominate the equilibrium, $Q_A^-Q_B \longleftrightarrow Q_AQ_B^-$.

The appearance of Q_A^- or Q_B^- induces pK_a shifts in ionizable groups, equivalent to the electrostatic interaction energy. In general, the magnitude of the response will fall off with distance, both because of the inherent distance dependence of charge-charge interactions and because the effective dielectric constant of the protein tends to increase with distance (28-31). In spite of the fundamentally flawed nature of the concept, effective dielectric constants have commonly been estimated from the apparent interaction energy between charged groups, as implied by the effects of mutations of ionized residues (20, 32-35). Values obtained for this region of the RC are in the range ε_{eff} = 25-40, implying that substantial pK_a shifts are expected only for nearby (or otherwise closely coupled) ionizable groups, if such groups exist. On the other hand, larger numbers of groups might be expected to experience small shifts.

Net H^+ uptake or release by an ionizable group will only occur to the extent that the shift in pK_a changes

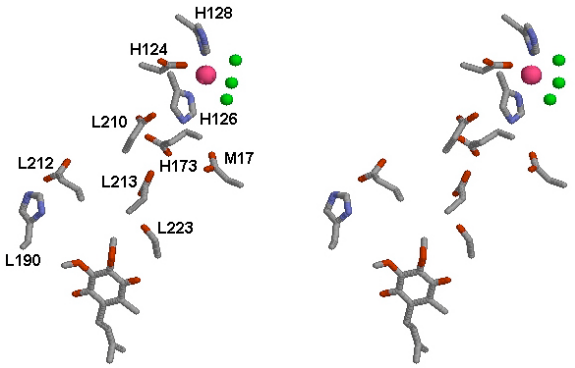

Figure 3. The acid cluster in the Q_B domain (cross-eyed stereo view). The orientation is within 30° of that in Figure 2 (top panel), but Q_B is in its distal position. The strongly interacting acid residues are Asp^{L210}, Glu^{L212}, Asp^{L213} and Glu^{H173}. Also shown is the inhibitory cadmium (Cd^{2+} - pink) binding site - Asp^{L124}, His^{L126}, His^{L128}, and 3 water molecules (green). Asp^{M17} is surface exposed and plays an important role in proton entry; it also coordinates to nickel (Ni^{2+}) when present. Coordinates are from 1ds8.pdb.

the equilibrium ionization state by a significant amount. Thus, it must be expected that the large majority of groups involved in net H^+ uptake or release will have pK_a values within, say, ± 1 unit of the ambient pH. (Groups with pK_a values outside this range will remain either fully protonated or fully deprotonated in either electronic state.) For such weakly coupled systems, proton uptake at a fixed pH can only be a minor contributor to the energetics of charge compensation. Although H^+ redistributions can contribute to the major dielectric response, the proton uptake is essentially only reporting such relaxations, rather than effecting them.

As the electron transfers from Q_A^- to Q_B, the protein dielectric will readjust to the new position of the electron charge. Surprisingly, but informatively, the H^+ uptake response of the RC protein is quite similar for Q_A^- and Q_B^-. The H^+/Q_A^- and H^+/Q_B^- stoichiometries are almost identical near neutral pH, and their pH dependences are qualitatively similar (19, 36), so net H^+ binding at a single pH contributes negligibly to the stabilization of Q_B^-. However, H^+ uptake to Q_B^- is somewhat larger at pH > 8 and pH < 6.5, i.e., b > a for the following reaction:

$$Q_A^- Q_B (H^+)_a \xleftrightarrow{L_{AB}^{(1)}} Q_A Q_B^- (H^+)_b \qquad \text{Scheme 2}$$

where $L_{AB}^{(1)}$ is the one-electron equilibrium constant. The small differences in H^+ uptake by Q_A^- and Q_B^-, integrated over the whole pH range, i.e., applying Eqn. 1, provide the net thermodynamic drive for the electron transfer equilibrium to lie in the forward direction at all pH < 11 (in isolated RCs from *Rba. sphaeroides)* (19).

Although the energies involved with H^+ events are small, they are functionally very important, as they modulate small values of the equilibrium between oxidized and reduced Q_A, where the latter is photochemically inactive [footnote1]. Thus, the quantum yield of primary events on the second flash can be easily changed from viable to non-viable values by quite subtle changes in the position of the $Q_A^-Q_B \longleftrightarrow Q_AQ_B^-$ equilibrium.

The similarity of the H^+ responses to Q_A^- and Q_B^- is given a clear mechanistic basis by electrostatic calculations on the RC structure (37, 38), which indicate that many of the same groups experience the bulk of the conformational changes and pK_a shifts in spite of the different locations of the semiquinone charge, and by the fact that all are closer to the Q_B site. This is because the local dielectric around Q_A^- is rather ineffective in screening the charge. Alexov and Gunner (37) suggested that the arrival of the electron on Q_A "prepares" the Q_B site for the subsequent electron transfer - an indication of apparent linkage between the two sites (see below, Section 5.4.4).

Many of the residues responsive in calculations were originally identified in mutant RCs as being important in the pH dependence of the rate ($k_{AB}^{(1)}$) and equilibrium ($L_{AB}^{(1)}$) constant for transfer of the first electron, as well as in the delivery of H^+ ions to the quinone headgroup on the second turnover. Experimental results from *Rba. sphaeroides* and *capsulatus* have suggested substantial, and even specific, roles for Glu^{L212} and Asp^{L213}, amongst others [footnote2] (33, 39, 40). However, computational studies show that the electrostatic interactions between groups in this region of the RC are so strong that ionization equilibria cannot be considered the property of individual groups, but are distributed over several members of an extensive, interacting cluster (41-44). Furthermore, while single mutation studies have often imputed great functional significance to individual residues, second site revertants have shown some of these to be non-unique solutions for functionality [footnote3]. For example, mutation of Asp^{L213} causes drastic failure of electron transfer and proton uptake to Q_B (33, 40, 45), but a second site revertant, Asn^{M44}–›Asp, restores function to a high degree (46). In fact, the combinations of Asp^{L213}/Asn^{M44} and Asn^{L213}/Asp^{M44} are equally functional in nature, and the latter is naturally encountered in *Rhodopseudomonas (Rps.)* (newly named *Blastochloris (Bcl.)) viridis*, *Rhodospirillum (Rsp.) rubrum* and *Chloroflexus (Cfl.) aurantiacus*, for example (47-50).

5. THE FIRST ELECTRON TRANSFER: $Q_A^-Q_B \longrightarrow Q_AQ_B^-$

5.1. Equilibrium

The one-electron equilibrium constant, $L_{AB}^{(1)}$, is roughly pH independent between pH 6 and 8, but increases at lower pH and decreases at higher pH (reviewed in (20)). This is generally interpreted as indicating the influence of the electric potential created by ionizable residues in the vicinity of Q_B, especially those comprising a cluster of interacting acidic residues, Asp^{L210}, Glu^{L212}, Asp^{L213}, and Glu^{H173} (Figure 3). Although the assignment of specific residues to observable phenomena may be naive, it retains some descriptive utility. For example, Glu^{L212} was suggested to be primarily responsible for the pH dependence of the first electron transfer, at pH > 8.5; it was

proposed to be neutral at pH < 8.5 and to become ionized with pK_a ≈ 9.8 (39). Some calculations show Glu^{L212} to undergo no changes in ionization state, and place all the burden elsewhere in the cluster, but FTIR studies have established that Glu^{L212} does indeed undergo changes in partial ionization, but differently so in many mutants (51-54). These results exemplify the complex interactions in this region of the protein.

Whatever the details, electron transfer to Q_B is inhibited by negative charge in the acid cluster, or "Glu^{L212}", which increases as it ionizes with an apparent pK_a ≈ 9.8 (p$K_{QA\text{-}QB}$ in Scheme 3) (33, 39, 55). Thus, the electron transfer equilibrium is apparently modulated by the equilibrium protonation state of $Glu^{L212}H/Glu^{L212}(-)$. For a single group titration, the apparent equilibrium constant, $L_{AB}^{(1)}$, progresses from a maximum value at low pH ($L_{AB}^{(1)'}$) to a minimum at high pH ($L_{AB}^{(1)o}$) (Scheme 3). In isolated RCs, $L_{AB}^{(1)}$ decreases steadily above pH 8.5-9 (corresponding to the onset of ionization, p$K_{QA\text{-}QB}$) and is pH dependent to above pH 11, so the apparent pK_a for Glu^{L212} with the electron on Q_B (pK_{QAQB}-) is ill-defined.

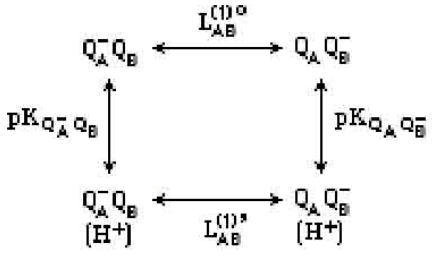

Scheme 3

In the dark adapted or ground state (Q_AQ_B), "Glu^{L212}" ionizes according to a lower apparent pK_a (pK_{QAQB}). Light activation causes proton uptake as the acid cluster reprotonates in accordance with the pK_a shifts induced by the semiquinone anions. The pH dependence of the H^+-uptake stoichiometries, H^+/Q_A^- and H^+/Q_B^-, can be deconvoluted into discrete contributions. If these are assigned to individual groups, the responses correspond to pK_a shifts of ≈ 1-1.6 units for 2-3 groups, of which "Glu^{L212}" is a major contributor with pK_{QAQB} ≈ 9-10 (18, 19, 36, 56, 57). Although this value is entirely dependent on this "discrete residue" model, when Glu^{L212} is mutated to a non-ionizable residue, light-induced proton uptake is eliminated at pH > 8.5, for both Q_A^- and Q_B^- (58, 59). This is consistent with electrostatic calculations, and illustrates the potential for long range interactions between the two quinone sites, including the proposed preparation of the Q_B site for the subsequent electron transfer from Q_A^- (37).

The pH dependence of $L_{AB}^{(1)}$ at pH < 6 was suggested to reflect the ionization behavior of Asp^{L213}, with pK_a ≈ 5 (33, 40). Calculations also roughly support this identification, but the behavior of Asp^{L213} is thought to be more complicated than this and involves a strongly coupled response of Asp^{L213} and Asp^{L210} (37, 60) (see Section 5.2).

The extensive nature of the ionization states in the RC are especially illustrated by one mutant in *Rba. capsulatus*. The loss of the high pH proton uptake to Q_A^- and Q_B^-, caused by the Glu^{L212}→Gln mutation, was substantially restored by a second site mutation in the Q_A binding pocket, Ala^{M247}→Tyr, more than 17Å away from Q_B (56). Remarkably, the functional pK_a value and the Q_B^--induced shift are similar to the wild type, but obviously cannot be associated with the residue at L212.

5.2. Electrostatic interactions in the quinone domains

The local electrostatic potential that acts on Q_B is the sum of many contributions, including a substantially positive potential from the peptide backbone (61) that is partially offset by the ionization of buried acidic groups [footnote4]. Against this background, the effects of mutations can be counter-intuitive. Thus, mutation of Asp^{L213} to Asn causes a dramatic increase in $L_{AB}^{(1)}$ and loss of pH dependence at pH < 6 (33). This is consistent with the removal of negative charge associated with ionized Asp^{L213} with pK_a ≈ 5, but the calculations of Alexov and Gunner (37, 60) show that the effect is more subtle and dynamic, as follows.

Because of the strong interactions between L210, L212, L213 and H173, charge sharing between them is hard to evaluate reliably. The calculations that allow conformational choices for polar residues and for the location of Q_B, show that (Glu^{L212} + Asp^{L213}) may best be considered as one group that is never more than singly ionized, at any pH (37, 38, 60, 62, 63). In the ground state (Q_AQ_B), there is a full charge on (Glu^{L212} + Asp^{L213}), and the OH group of Ser^{L223} is hydrogen bonded to Asp^{L213}. Asp^{L210} is protonated with an effective pK_a ≈ 9. In the $Q_AQ_B^-$ state, (Glu^{L212} + Asp^{L213}) becomes fully protonated by intraprotein proton transfer from Asp^{L210}. Also, the OH of Ser^{L223} switches to hydrogen bond with the carbonyl oxygen (O1) of Q_B^-, and the carboxylic OH of Asp^{L213} hydrogen bonds to the O_γ of Ser^{L223} (Figure 4). Because Asp^{L213} is now neutral, the pK_a of Asp^{L210} decreases significantly and is reprotonated from solution at pH < 7. At pH > 8.5, as Asp^{L210} becomes progressively more ionized in the ground state, the protonation of (Glu^{L212} + Asp^{L213}) after activation occurs by uptake from solution. This accounts, qualitatively, for the observed proton uptake.

To a first approximation, the central position of Asp^{L213} in strong interactions with Glu^{L212}, Asp^{L210} and Q_B^- gives rise to much of the observable protonation and pH dependent behavior associated with the first electron transfer. By virtue of proton transfer within the acidic cluster, Q_B^- induces an apparent pK_a shift from 5 to >13 for (Glu^{L212} + Asp^{L213}), while the pK_a of Asp^{L210} actually *downshifts* from 9 to 7 (Figure 5).

An interesting corollary of this scenario is that the charge on (Glu^{L212} + Asp^{L213}) does not directly influence the electron transfer equilibrium through electrostatic interaction with $Q_AQ_B^-$, because (Glu^{L212} + Asp^{L213}) is always neutral when Q_B^- is present (37, 38). Thus, the effect of the Asp^{L213}→Asn mutation, which greatly increases the one-electron equilibrium, is not simply due to a more positive potential at Q_B, but is exerted through the free energy of the $Q_A^-Q_B$ state (60). In Figure 4, the dominant equilibrium is between state A and state B'.

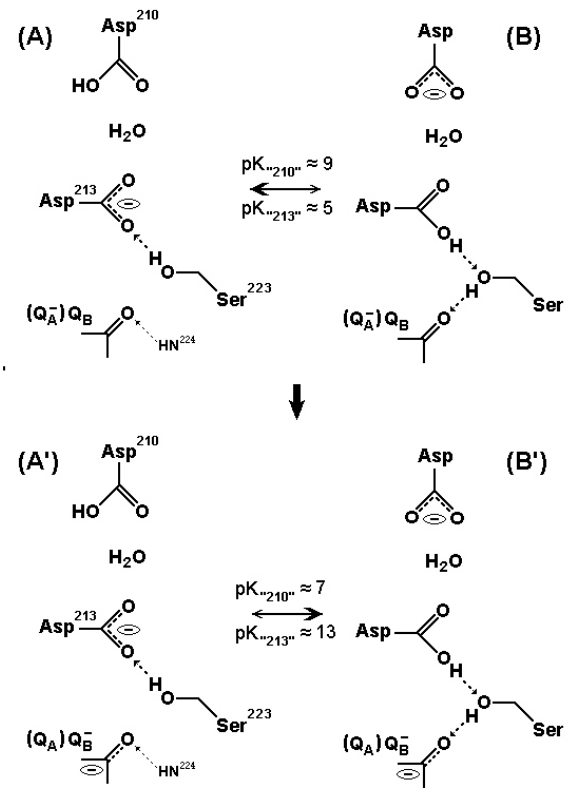

Figure 4. The Serine-L223 hydrogen bond switch. Top panel: in the $Q_A^-Q_B$ state (and in the Q_B(proximal) ground state), the equilibrium lies to the left (state A). Q_B is shown hydrogen bonded at the C1 carbonyl by the peptide nitrogen of residue L224. Asp^{L213} (Glu^{L212} + Asp^{L213} in the text) is ionized. This suppresses the ionization of Asp^{L210}, which is neutral. Ser^{L223} serves as a hydrogen bond donor to the carboxylate of Asp^{L213}. Bottom panel: upon reduction of Q_B, the individual pK_as of the acid cluster residues change dramatically and the equilibrium shifts to the right (state B'). Asp^{L213} becomes protonated, removing the electrostatic restraint on Asp^{L210}, which ionizes. The carboxylic OH of Asp^{L213} now donates a hydrogen bond to Ser^{L223}, which switches its hydrogen bond to donate to Q_B^-. This is probably an important contribution to the stabilization of the semiquinone state, substantially raising its redox midpoint potential (E_m) from solution values (ref. 4, and C.A.W., in preparation). The type of pK_a changes involved in this scenario is shown schematically in Figure 5.

In mutants lacking Asp^{L213}, the left hand side of Figure 4 is missing and the equilibrium is between states B and B' (60). An equivalent view might be that Q_B^- is stabilized by the hydrogen bond from Ser^{L223} which is competed for by Asp^{L213}. Thus, when this residue is mutated, the serine can give all its attention to the semiquinone.

Mutation of Glu^{H173} to glutamine results in inhibition of turnover comparable to that seen for Asp^{L213}–›Asn (64). However, in contrast to the latter mutation, Glu^{H173}–›Gln *decreases* L_{AB}[(1)], suggesting that the local potential at Q_B becomes *more* negative. This was proposed to be due to a compensating increase in negative charge appearing on other residues closer to Q_B, e.g., Glu^{L212} or Asp^{L213} (64). Electrostatic calculations support this interpretation (E. Alexov, personal communication). A similar, but much smaller, effect was reported for mutation of Arg^{L217}, which caused a counter-intuitive decrease in the pK_a of Glu^{L212} (35). This was interpeted as indicating a change in the "chemical proton affinity" of Glu^{L212}, or the local proton activity, of non-electrostatic origin. Although providing a simplified approach to modeling the outcomes, this seems to be an *ad hoc* way of accounting for the complex electrostatics of the system.

The fundamentally electrostatic nature of the influences in this region is reinforced by the restoration of function to Asp^{L213} (and Glu^{L212}) mutations by second-site revertants that add a negative charge elsewhere, especially Asn^{M44}–›Asp (46, 65), or a compensating removal of a positive charge, as in Arg^{M233}–›Leu or Cys (66, 67) or Arg^{H177}–›His (68). The long-range effects of some second-site reversion mutations are likely to be conformational in nature, albeit instigated by electrostatic perturbations. The implied structural perturbations can only be revealed by direct methods, and the Arg^{M233}–›Cys mutation, which is a second site revertant to both Asp^{L213} and Glu^{L212} lesions, has been analyzed by X-ray diffraction (69). A cascade of structural changes is seen to propagate from the mutation site, with small perturbations seen as far as Q_B, more than 15Å away. These include a significant shift in the position of Arg^{H177} and the introduction of a novel water molecule close to Glu^{H173} but not adjacent to Q_B ((69) and M. L. Paddock, personal communication). FTIR studies on this mutant also reveal extensive structural changes (70).

Site-directed mutagenesis and computational studies generally converge in identifying "important" residues, but calculations have been inconsistent on specific predictions of the ionization behavior of individual groups, e.g., Glu^{L212} has been variously found to be fully or partially charged or neutral (37, 38, 42, 71, 72). FTIR data, which seem to be on firm ground, show it to be partially ionized (51-54). The discrepancies probably reflect how sensitive the calculated responses of coupled residues can be to the input parameters, such as the intrinsic pK_a values [footnote5] for each residue, without significantly changing the net energetics.

In addition, some sites of protonation may be intrinsically ill-defined. FTIR studies found distinct changes in the carboxylic acid region above 1700 cm^{-1}, in *Rba. sphaeroides* but none in *Rps. viridis* (73, 74). This prompted a look for signatures of delocalized, "Zundel" protons in the light-induced difference spectra. Zundel has long proposed that protonation of strongly hydrogen bonded networks gives rise to highly polarizable systems that exhibit very broad band (hundreds of cm^{-1}) or continuum (thousands of cm^{-1}) IR absorbance (75, 76). IR difference spectra of the Q_A^- and Q_B^- states revealed broad band changes at ≈2700 cm^{-1}, in both *Rba. sphaeroides* and *Rps. viridis* RCs, that shifted to ≈2100 cm^{-1} in D_2O (77). While these results are highly suggestive, at the present time there is no way to quantitate the contribution of such

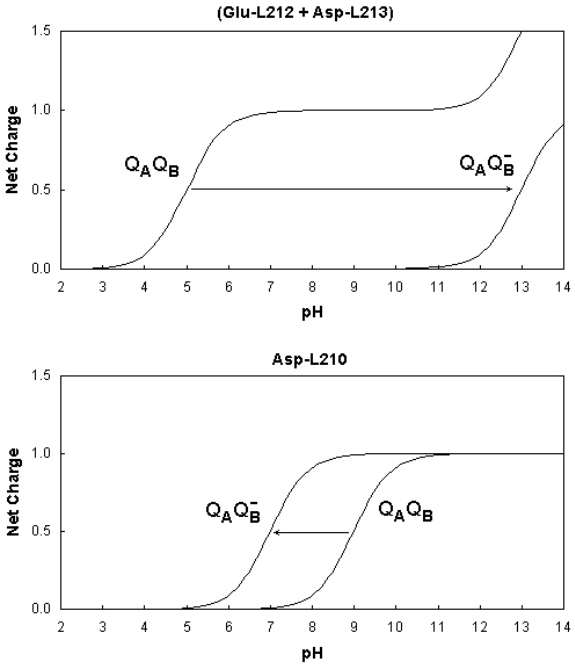

Figure 5. Schematic titration curves for key residues of the acid cluster in the ground state (Q_AQ_B) and one electron reduced state ($Q_AQ_B^-$), according to the electrostatic-molecular mechanics calculations of Alexov and Gunner (37). Note the counter-intuitive *downshift* in the pK_a of Asp^{L210} upon reduction of Q_B (see text).

protonation states. Similar IR bands are seen in bacteriorhodopsin (bR), associated with the "proton release complex" of the extracellular domain (78, 79). In the absence of any other identifiable signals in bR, the Zundel band is presumed to account for a full proton.

5.3. Kinetics

In addition to the decrease in the equilibrium constant, the rate of the first electron transfer, $k_{AB}^{(1)}$, also slows down at pH > 8.5, exhibiting a pK_a = 9.2-9.5, somewhat lower than the equilibrium value. However, no acceleration is apparent at low pH (< pH 6), where $L_{AB}^{(1)}$ increases, suggesting a change in rate limitation or control (20). The lower value for the alkaline pK_a, compared to the equilibrium value of ≈ 9.8, probably reflects its kinetic nature and the fact that the protonation state immediately after the flash is determined by the pre-flash (ground state) equilibrium, i.e., pK_{QAQB} ≈ 9, rather than pK_{QA^-QB}. The difference of 0.5-1 units between pK_{QAQB} and pK_{QA^-QB} indicates the electrostatic influence of Q_A^- on the apparent pK_a of "Glu^{L212}. This is seen directly in the pH dependence of the H^+/Q_A^- stoichiometry. Q_A^- has similar effects on subsequent turnovers, with pK_a shifts of 0.7-0.8 pH units estimated for the pK_a of the Q_B semiquinone (pK_s) in the 2-electron state $Q_A^-Q_B^-$, and for pK_1, the first pK_a of the quinol, QH^-, in the 3-electron state $Q_A^-Q_BH^-$ (80, 81). It is worth noting, however, that the distinction between kinetic and equilibrium pK_a values of the 1st ET, is greatly exaggerated in some mutations of key residues, especially those that dramatically affect the 2nd ET, e.g., Asp^{L213}→Asn (33), Glu^{H173}→Gln (64) and Asp^{H170}→Asn (82) (see section 5.4.4).

Because Q_A and Q_B are both ubiquinone (Q-10) in *Rba. sphaeroides*, with almost identical electronic spectra, monitoring the first electron transfer generally relies on the differential electrochromic effects of Q_A^- and Q_B^- on the neighboring chlorins (Bphe and Bchl) (83, 84). This allows for other charge movements, including proton transfers and conformational motions, to contribute to the overall kinetics, which are also wavelength-dependent, reflecting local contributions to the responses of different chromophores (85-87). Wraight and coworkers (88, 89) reported the kinetics at 397 nm (the Soret region of Bphe) to be biphasic, with both components exhibiting pH dependent rate constants - a fast phase with τ ≈100 μs, and a slow phase with τ ≈ 1 ms. The relative amplitudes of these phases did not vary as the extent of Q_B activity was increased, suggesting that both components arose from a single occupancy quinone binding with two configurations of different reactivity (89) (P. Maróti and C.A. Wraight, unpublished). Measuring in the Q_y bands of Bphe and Bchl, Tiede *et al.* (87) reported complex (dispersive), and generally faster, kinetics. The spectral response at 757 nm appeared to be the positive lobe of a bandshift of Bphe, but the negative component at 770 nm exhibited quite different kinetics. This is a bizarre effect that is not understood at the present time, but Tiede *et al.* concluded that the 757 nm transient is a reliable monitor of the $Q_A^-Q_B$ ⟶ $Q_AQ_B^-$ electron transfer event, which is at least biphasic, while other wavelengths include various responses to other factors, such as proton transfer.

5.4. Possible structural bases of the 1st electron transfer

5.4.1. The proximal/distal positions of Q_B

The kinetic complexity of the first electron transfer was given additional significance by the discovery that, at least in crystals of isolated RCs, Q_B may not normally be *in* the Q_B pocket at the time of reduction of Q_A^-. In dark-adapted RC crystal structures, the natural, long-chain ubiquinone species do not occupy the functional (also termed *proximal*) Q_B binding site, but bind preferentially at the threshold of the pocket, in a *distal* position (90, 91) (compare Figures 3 and 7). Graige *et al.*, who also observed biphasic kinetics in the 1st ET, found that neither rate was dependent on the driving force of the reaction (ΔG^o), which was varied by employing non-native (naphtho)quinones with different redox potentials as Q_A, but with Q-10 as Q_B (92). They concluded that the rate limiting process was not electron transfer and proposed that movement of quinone from the distal to proximal Q_B binding site constituted a type of conformational gating.

Electrostatic and molecular dynamics/mechanics simulations that include the distal site configuration suggest that the protonation state changes induced by Q_A^- are sufficient to tip the binding equilibrium to favor entry of ubiquinone into the proximal site (38, 93-95). It would then be effectively nailed into position by transfer of the electron. However, X-ray structures show that RCs with the mutation Pro^{L209}→Tyr have Q_B already in the proximal site (96), but exhibit no significant differences in the 1st

electron transfer kinetics (97). Thus, the quinone movement, *per se*, does not appear to be rate limiting, even though an energetically quite expensive ring flip is required for the quinone headgroup to reach its final, proximal orientation (90, 94). Furthermore, FTIR studies have failed to detect the distal position in functional turnover of the Q_B site, even in wild type RCs (98). This is, therefore, an open question at the present time.

In fact, at pH ≤ 8, the time scale of the 1st electron transfer is similar to that of H^+ uptake to the Q_A^- state, alone, for which no quinone motion is required (26). At pH > 8.5, electron transfer to Q_B is retarded by the need for additional proton uptake to neutralize "Glu^{L212}". However, proton uptake does not appear to be rate limiting either (see Section 7.2.1), although it may be instrumental in preparing the Q_B site energetically, which could include bringing the headgroup into the proximal position. The overall reaction could, perhaps, be rate limited by protein dynamics that limit both H^+ uptake and electron transfer and pull the equilibrium over to an observable extent. As discussed above, *net* proton uptake accompanying or following electron transfer cannot be responsible for the equilibrium position as there is little difference between the H^+/Q_A^- and H^+/Q_B^- stoichiometries, but protein relaxations including H^+ ion redistribution and *indicated* by H^+ uptake, are a possibility.

5.4.2 The role of quinone binding in the overall 1st ET equilibrium

Although the pH dependence of the 1st ET equilibrium is generally considered to reflect electrostatic influences on the electron transfer, *per se*, i.e., $Q_A^-Q_B \leftrightarrow Q_AQ_B^-$, Takahashi *et al.* (99) reported that the affinity for Q-0 in the Q_B site was pH dependent in a manner identical to the overall ET equilibrium, and similar results were found with Q-10 (C.A.W., unpub.). This could account for essentially all of the pH dependence of the observed ET equilibrium. The observed equilibrium constant is an *apparent* one that includes saturation of the binding site, described by an association constant, K_Q, which was found to be pH dependent:

$$L_{AB}^{app} = L_{AB}^{(1)} \frac{K_Q[Q]}{1+K_Q[Q]} \qquad \text{Eqn. 2}$$

In order for the pH dependence of K_Q to show up in L_{AB}^{app} (for a single step quinone binding), the binding must not be saturated. However, Shinkarev and Wraight (100) have shown that the statistical distribution of quinone in detergent suspension makes true saturation much more difficult to achieve than previously recognized.

In fact, a 2-step binding equilibrium, such as implied by the proximal/distal description, adds an intrinsic restriction to achieving saturation, and the binding picture would now look like:

$$Q_A(\ldots) + Q \xrightleftharpoons{K_q} Q_A{\bullet\bullet}Q_B \xrightleftharpoons{K_b} Q_AQ_B \qquad \text{Scheme 4}$$

Where $Q_A(...)$ indicates no occupancy of the Q_B pocket and $Q_A{\bullet\bullet}Q_B$ represents Q_B binding in the distal position. Omitting the complexities of detergent/quinone distributions (100), the net affinity (association constant) is given by: $K_Q = K_q(1 + K_b)$. The apparent ET equilibrium will reflect this and, even at saturating levels of quinone, is given by: $L_{AB}^{app} = L_{AB}^{(1)}.K_b/(1 + K_b)$. Provided K_b is not large, its pH dependence will show up directly in L_{AB}^{app}. Various computational studies have indicated that the proximal/distal distibution is, indeed, dependent on the protonation state of various residues (38, 93-95).

Occupancy of the functional Q_B position (the proximal-distal equilibrium) is likely to be determined by competition between water and quinone in the proximal Q_B site. X-ray structures of RCs show several (up to 6) water molecules in the Q_B site, when Q_B is absent (91). With Q_B in the distal site, 2-3 water molecules may remain in the proximal site, possibly hydrogen bonded between Glu^{L212} and His^{L190} (90, 91, 101). Water is held exclusively by electrostatic interactions (including hydrogen bonds) within the pocket, whereas the quinone interactions are predominantly van der Waals, plus hydrogen bonds to the carbonyl oxygens and possibly the C3' methoxy oxygen. Thus, the water should be harder to displace at high pH as more ionization occurs in the Q_B region. Tiede *et al.* (87) and Larson and Wraight (102) found that the 1st ET accelerates in high osmotic strength media, consistent with an enhanced occupation of the proximal site.

5.4.3. Fast phases of the 1st ET

Although the rate of the first electron transfer exhibits no dependence on the free energy on time scales greater than ≈10 µs, Li *et al.* have reported a faster component that *is* dependent on ΔG^o (103, 104). This was only observed for low potential naphthoquinones as Q_A. Graige *et al.* (92) did not see it, albeit with different conditions, but may have since reported it at low pH (105). It was also not seen with ubiquinone as Q_A in a mutant that invests the native quinone with a low potential, although it was again observed with naphthoquinones (104). The fast phase, therefore, seems to be very sensitive to conditions, which may indicate that it reflects a delicately balanced proximal-distal equilibrium in the dark that can tip either way, depending on influences such as detergent or membrane [footnote6] environment, osmotic strength, changes in the quinone structure in the Q_A site, and mutations. Once the proximal position is dominant, the role of other processes in the net reaction can be seen, including electron transfer, as suggested by the ΔG^o dependence observed by Li *et al* (104).

On this basis, the data of Li *et al.* indicate that even when Q_B is present and able to be reduced by Q_A^- on the 1 µs time scale, it is energetically unfavorable unless the equilibrium is artificially enhanced by using sufficiently low potential analogues of Q_A. The result is that both the amplitude and the rate of the fast phase increase with driving force. The Q_A redox potential necessary to produce 50% fast phase (indicating an initial equilibrium constant of 1) is about 100 mV more negative than that of ubiquinone. This would mean that for wild type RC with native Q_A, even after preparation of the Q_B site and migration of quinone into the proximal position, the initial electron transfer to Q_B is still unfavorable, and the equilibrium must

be pulled over by subsequent events that stabilize Q_B^-, i.e., relaxations, which may include H^+ redistribution and the Ser^{L223} -OH flip. The analysis of Gunner and coworkers (104) suggested a reorganization energy of about 0.9 eV for the 1st ET reactions with naphthoquinone as Q_A. This is significantly smaller than estimates for the 2nd ET (see below) and could be considered consistent with electron transfer preceding H^+ uptake, and therefore less dependent on significant charge rearrangements.

5.4.4. Linkage between Q_A and Q_B

Many examples exist of apparent interaction between the two quinone sites, and are often evident in pH dependences and protonation behavior. Such mutual influence or linkage (4, 106) includes the long-known response of the E_m of Q_A and its redox-linked pK_a (pK_{QA}-) to the occupancy of the Q_B site by inhibitors (107, 108) and quinone/quinol (109), as well as the long-distance influence of Q_A^- on the ionization and conformational responses of acidic groups near the Q_B site, as described above. One of the most striking and relevant examples of long range influence is the great reduction and even elimination of the high pH proton uptake to the Q_A^- state when certain naphthoquinones are substituted for the native ubiquinone (Q-10) in the Q_A site (110). Since H^+ uptake in this pH region is largely identified with the acid cluster of the Q_B pocket, this suggests the signaling of structural information from one site to the other. Conceivably, isoprenyl ubiquinones impose some strain (111) that is relayed to the Q_B domain to induce the protonation/conformational configuration that favors the distal position for Q_B. In contrast, the planar naphthoquinones could allow a small structural relaxation that tips the balance in favor of proximal site occupancy.

Interactions between the Q_A and Q_B sites are also evident in the effects of certain mutations. Substitution of Ile^{M265}, in the Q_A site, with polar residues threonine and serine causes a dramatic lowering of the E_m of Q_A, and also introduces a novel pK_a in the kinetics of the 1st ET (112). The behavior of the Q_A site mutation, Ala^{M247}→Tyr, as a second site revertant that restores the wild-type pattern of H^+ uptake in the Glu^{L212}→Gln mutant (56), has not been reported as a single site mutation but will be very interesting to see.

Many other mutations appear to amplify the distinction between apparent pK_a values operative in the kinetic, compared to equilibrium, properties of the 1st ET. In such cases, the rate of electron transfer becomes pH dependent at much lower pH than does the equilibrium constant (33, 64, 82). This is consistent with conformational control of the kinetics - for example, with distinct pK_a values for functional binding of Q_B in the proximal position and for the electron transfer, itself. The exaggerated distinction between kinetic and equilibrium pK_a values seen in some mutants could then indicate slower kinetics of the conformational change. A general model of this behavior has been described, including such pK_a distinctions (106). It was suggested that rapid electron and proton transfers establish an initial equilibrium, which strongly disfavors $Q_AQ_B^-$ and may, therefore, be undetectable with the normal driving force available from ubiquinone as Q_A. Subsequent rate-limiting and proton-linked conformational changes determine both the attainment of the final equilibrium and at least some of the observable H^+ uptake.

A specific model of Mulkidjanian and coworkers (35, 113), based largely on electrometric measurements in chromatophores, proposes Glu^{L212} to have a much lower p$K_a \approx 6$ when quinone is not in the proximal position, due to the H_2O that is present instead. This low pK_a value is not obviously consistent with the pH dependence of the H^+/Q_B^- stoichiometry in isolated RCs, which does not support the implied large shift in pK_a from 6 to >11. Nor is it readily reconciled with the specific loss of H^+ uptake at high pH (>8.5) when Glu^{L212} is mutated. Furthermore, the mutant Pro^{L209}→Tyr, which appears to have Q_B already in the proximal position in the ground state (96), has very similar H^+/Q_B^- stoichiometry to the wild type, across a wide pH range (57). This, in particular, is inconsistent with substantially different pK_a values of key residues for the distal vs. proximal positions of Q_B. However, it can be added that the inevitable electrostatic interactions within the acid cluster render these criticisms equivocal.

As seen when naphthoquinones are used as Q_A, some mutations appear to "break" the linkage between the two quinone sites, as assayed by Q_A^--induced H^+ uptake at high pH, which is largely ascribed to the acid cluster near Q_B. Most notable of these are mutations of Pro^{L209} to Phe, Tyr and Trp (57, 97, 114), which have also been characterized by X-ray diffraction analysis. From these, an interesting candidate for the linkage effect is a cluster of water molecules, originally identified by Fritzsch (115), which almost extends from one quinone site to the other. Since it is sufficiently ordered to be well defined in the X-ray structure, it might also function as a polarizable transmitter of the electric potential of Q_A^- to the acid cluster.

6. THE SECOND ELECTRON TRANSFER: $Q_A^-Q_B^-$ —› $Q_AQ_BH_2$

Transfer of the second electron to Q_B is tightly coupled to delivery of the first proton (H_I^+) to the quinone headgroup. This can occur in one of two sequences, with electron transfer preceding (ET/PT) or following (PT/ET) proton transfer (85), both proceeding *via* energetically unfavorable intermediates, $Q_A^-Q_BH$ or $Q_AQ_B^{2-}$:

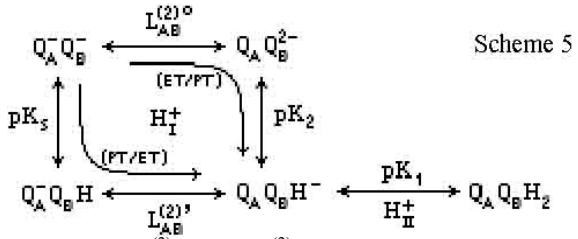

Scheme 5

Here $L_{AB}^{(2)o}$ and $L_{AB}^{(2)'}$ correspond to the limiting equilibrium constants for electron transfer at high and low pH, i.e., above pK_2 and below pK_s, respectively. Note that the first proton taken up (H_I^+) corresponds to what is normally defined as the second ionization of the quinol

(pK_2), and the second proton taken up H_{II}^+) corresponds to the first ionization (pK_1).

The energetic accessibility of the intermediates for the two possible pathways of coupled proton-electron transfer (PT/ET vs. ET/PT) depends on the pK_a of the Q_B semiquinone (pK_s) and on the degree of stabilization of the Q_B^{2-}/Q_B^- redox couple. The range of values for pK_s (≈ 5 in water, and 4-6 in RCs (81, 116)), suggests that the $Q_A^-Q_BH$ state lies 60-180 meV above $Q_A^-Q_B^-$, at pH 7, but progressively more at higher pH (ideally 60 meV per pH unit). Although the likely range for $E_m(Q_B^{2-}/Q_B^-)$ places $Q_AQ_B^{2-}$ at least 240 meV above $Q_A^-Q_B^-$ (C.A.W. - in preparation), this should be pH-independent and the two routes are not clearly distinguished on purely energetic grounds. However, distinction between the two pathways was made by Graige *et al.*, who found that the rate of the observed second electron transfer, $k_{AB}^{(2)}$, is dependent on the driving force for the reaction, set by varying the redox potential of Q_A with quinone analogues (117).

Analysis of the free energy and pH dependences of the rate provided strong evidence that the reaction mechanism proceeds *via* rapid pre-protonation of the semiquinone followed by rate-limiting electron transfer (the lower, PT/ET route in Scheme 5), i.e., the neutral semiquinone is a transition intermediate (117). The energetics are shown in Scheme 6. The value of pK_s controls the population of Q_BH, which determines the height of the intermediate state, and sets the functional E_m of the Q_BH^-/Q_BH redox couple, which determines the actual free energy of the electron transfer step, $\Delta G_{ET}^{(2)}$. Both contribute to the observed rate, $k_{AB}^{(2)}$.

Scheme 6

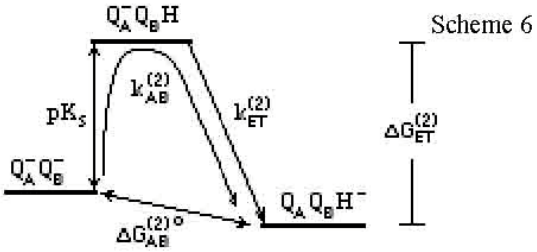

Proton transfer is apparently fast enough to establish Q_BH in an equilibrium population determined by pK_s and the ambient pH. Thus, the observed rate is $k_{AB}^{(2)} = k_{et}^{(2)} f(Q_BH)$ and, for a simple titration, $f(Q_BH) = 10^{pK_s\text{-}pH}/(1+10^{pK_s\text{-}pH})$. Since ET is rate limiting over the accessible pH range, from pH 4-11 (117), the proton transfer equilibrium must be established at least 10 times faster, at all pH. Exactly how fast the ET rate is, and therefore how fast the PT rate must be, depends on the functional pK_s of the Q_B semiquinone.

6.1 The Q_B semiquinone pK_a (pK_s)

Following the first electron transfer, the spectrum of the photoproduct in isolated RCs indicates that the Q_B semiquinone remains fully anionic at least down to pH 3.5 (85, 118), implying $pK_s \leq 3$ for the $Q_AQ_B^-$ state. However, if such a pK_s value were straightforwardly applicable to $Q_A^-Q_B^-$ after the 2nd flash, then the rate of reaction, by the PT/ET mechanism, would be very pH dependent (ideally a 10-fold change in rate per pH unit). In fact, for wild type RCs, the rate of the 2nd ET is at a maximum or plateau below pH 4.5 ($k_{AB}^{(2)}$ = 2-5 x 10^4 s^{-1}), decreases slowly between pH 4.5 and 8, and more steeply only at pH > 8 (85).

Also, if Q_BH exhibited simple titration behavior, the plateau would indicate that pK_s lies above pH 4. In fact, the weak pH dependence up to pH 8 suggests that pK_s is not constant but is continuously modulated by interactions with a changing electrostatic environment that keep the functional pK_a below the prevailing pH. Even if Q_BH were fully titratable in the $Q_A^-Q_B^-$ state at sufficiently low pH, direct proof of this, such as by spectroscopic identification, is likely to be difficult as Q_BH is expected to be very rapidly reduced to Q_BH^-. However, by using rhodoquinone (RQ) as Q_B, Graige *et al.* found that $k_{AB}^{(2)}$ showed a clear dependence on the equilibrium population of Q_BH (81). This 3-amino-analogue of ubiquinone has a much higher solution pK_s (≈ 7.5). With RQ as Q_B, protonation of the semiquinone was observed directly in the one electron state, $Q_AQ_B^- \leftrightarrow Q_AQ_BH$, with $pK_s \approx 7.2$. On the second electron transfer, $k_{AB}^{(2)}$ displayed a well-behaved pH dependence, decelerating 10-fold per pH unit above a pK_s of 8.0 in the $Q_A^-Q_B^-$ state. The 0.8 unit upshift in pK_s in the $Q_A^-Q_B^-$ state is similar to that inferred for the normal ubiquinone occupant (80). Comparison of the behavior of RQ with that of UQ as Q_B, suggested an apparent pK_s = 4.5-5 for native ubiquinone in $Q_A^-Q_B^-$, at pH 7.5. This is very similar to the pK_a estimated for ubisemiquinone in water (pK_a = 4.9; C.A.W., unpub.). Establishing $pK_s \approx 4.5$ determines both $\Delta G_{ET}^{(2)}$ and $k_{ET}^{(2)}$, which then sets the lower limit on the rate of proton equilibration, $k_{eq} = k_{on} + k_{off}$.

6.1.1 Energetics and kinetics of the proton coupled electron transfer

The driving force for the electron transfer step, $\Delta G_{ET}^{(2)}$, depends on the redox potential of the transition intermediate, Q_BH^-/Q_BH. For $pK_s \approx 4.5$ and $pK_1 \approx 8.5$ (see Section 6.3), we can estimate $E_m(Q_BH^-/Q_BH) \approx +0.21$ V (C.A.W., unpub.) and hence obtain $\Delta G_{ET}^{(2)} = -(E_m(Q_A^-/Q_A) - E_m(Q_BH^-/Q_BH)) \approx -0.255$ eV. Also with pK_s = 4.5, the measured value of $k_{AB}^{(2)} = 3 \times 10^3$ s^{-1} at pH 7 gives $k_{ET}^{(2)} \approx 10^6$ s^{-1}, as deduced by Graige *et al.* (81).

In the high temperature limit, the classical Marcus equation and the quantum mechanical version are the same:

$$\ln k_o/k = \frac{(\Delta G^0 + \lambda)^2}{4k_B T\lambda} \qquad \text{Eqn. 3}$$

where k_o is the maximum rate obtained when the free energy of reaction ($\Delta G°$) and the reorganization energy (λ)are equal and opposite, $\Delta G° = -\lambda$. The maximum rate is determined only by the electronic coupling and the distance between the electron acceptor and donor: $k_o = A.\exp(-\beta R)$. The edge-to-edge distance from Q_A to Q_B in the proximal position (≈14.5 Å), and the unusually strong electronic coupling between the quinones, give a maximum rate $k_o \approx$ 1-3.5 x 10^9 s^{-1} (119-121). Inserting $k_{ET}^{(2)} \approx 10^6$ s^{-1} and $\Delta G_{ET}^{(2)} \approx -0.25$ eV into the Marcus equation, with $k_o = 3 \times 10^9$ s^{-1}, we obtain a reorganization energy, $\lambda \approx 1.3$ eV, for the classical form of Eqn. 3 [footnote7]. This is well within the

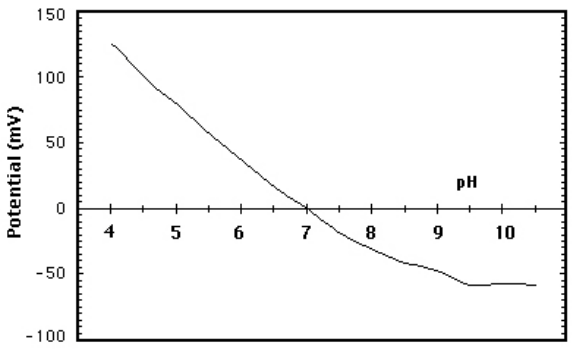

Figure 6. pH dependence of the effective electrostatic potential at the Q_B site in the $Q_A^-Q_B^-$ state. The potential was calculated on the assumption that the pH dependence of the rate of the 2nd electron transfer, $Q_A^-Q_B^- \rightarrow Q_AQ_BH^-$, is determined by the p$K_a$ of the Q_B^- semiquinone. The experimental rate is then compared with the expected titration of a single, non-interacting site, according to the Henderson-Hasselbalch equation, with pK_a = 4.5 (see text). The position of the curve on the vertical scale is somewhat arbitrary, and moves with the choice of a reference pK_a value, but the extent of the change (150-200 mV) over the range pH 4 - 9 is essentially unaffected.

range of values considered appropriate for ET involving the Q_B site, e.g., as estimated for charge recombination from the $P^+Q_B^-$ state (125, 126). Dutton and coworkers have recommended that some residual quantized behavior be included in typical biological ET reactions, yielding a factor in the denominator of Eqn. 3 of about 0.14, rather than $4k_BT \approx 0.1$ eV (122, 128). This results in $\lambda \approx 1.6$ eV, which is likely too large. Almost as high a value was suggested by Schmid and Labahn (127), but is better accounted for by at least some, and probably substantial, temperature dependence of the free energy, ΔG^o (25).

In the PT/ET mechanism for the second electron transfer, *via* Q_BH, the protonation equilibrium must be established faster than the forward rate of electron transfer, i.e., $k_{eq} = k_{on} + k_{off} > k_{ET}^{(2)} > 10^6$ s^{-1} (68, 81). For equilibrium from the bulk phase, the on-rate is pH dependent, $k_{on} = k_H.10^{-pH}$, where k_H is on the order of 10^{11} M^{-1} s^{-1}, while the off-rate is determined (ideally) by the pK_a of the reactive species (Q_B^-/Q_BH), $k_{off} = k_H.10^{-pK_s}$ (129, 130). For $k_{eq} > 10^6$ s^{-1} over the whole experimental pH range, and with $k_H = 10^{11}$ M^{-1} s^{-1}, we find $k_{on} > 10^6$ s^{-1} only at pH < 5. On the other hand, $k_{off} > 10^6$ s^{-1} with pK_s < 5. Thus, the requirement for $k_{eq} > k_{ET}^{(2)}$ must be largely satisfied by a low pK_a value for Q_B^-, and we can consider the derived value of 4.5-5 to be consistent with this assessment.

6.1.2 pH dependence of pK_s

A value of pK_s in the range 4.5-5 would place it right in the middle of the carboxylate pK_a range, where the protein electrostatics are most complex. In contrast, the pK_s for RQ lies outside this range. Lavergne *et al.* found that protonation of the stable Q_B ubisemiquinone ($Q_AQ_B^-$) is readily observable in chromatophores, with a functional pK_s = 6 (116). Rather than being indicative of a major difference between chromatophores and isolated RCs, however, this may simply suggest that the point at which pK_s approaches and exceeds the ambient pH (thereby allowing significant levels of Q_BH) can depend on minor changes in the intrinsic pK_a values of Q_B^- and the amino acids involved, and on their strengths of interaction, both likely sensitive to the environment, e.g., detergent *vs*. membrane. In addition to the functional pK_a for Q_B^-, other differences may exist between isolated RCs and chromatophores. A striking example is the fact that $E_m(Q_A^-/Q_A)$ is strongly pH-dependent in chromatophores (108) but not in isolated RCs (109, 131, 132). However, recent determinations of the free energy gap between P* and $P^+Q_A^-$ in chromatophores reveal an identical pH dependence to that seen in isolated RCs and cast serious doubt on the potentiometric measurements of $E_m(Q_A^-/Q_A)$ (C.A.W., in preparation).

Computational analyses of protein electrostatics readily show the effects of interaction between ionizable residues on their pK_a values, as in the acidic residue cluster around Q_B (37, 42, 44, 133, 134). However, it is perhaps unexpected that the pH dependence of $k_{AB}^{(2)}$ is of almost identical form (curvature) for a wide variety of mutants in and around the Q_B domain (68, 134-137). This suggests that in the $Q_AQ_B^-$ and $Q_A^-Q_B^-$ states, when (Glu^{L212} + Asp^{L213}) is neutral, no single strong interaction determines the functional pK_a of Q_B^-, but that the effective potential at Q_B is the sum of many smaller contributions. By comparison of the experimental data (rate *vs*. pH) with the pH dependence expected for a simple titration, we can estimate the pH dependent changes in the local potential ($\delta\Psi$), which modulate the actual pK_a:

$$k^{obs} = k_{max}/(1 + 10^{pH-pK_s+\delta pK})$$
$$\delta pK = -\delta\Psi/2.303RT \qquad \text{Eqn. 4}$$

Assuming pK_s = 4.5, the local potential is zero at about pH 7 (Figure 6). Regardless of the choice of pK_s, the potential drops by about 180 mV from pH 4 to 9 and then flattens out. Although this is a large decrease, it is comparable to what is obtained from a full protein electrostatics calculation (E. Alexov, personal communication).

6.2 The energetics of the overall 2nd ET reaction

The value of pK_s establishes the operational E_m of the Q_BH^-/Q_BH redox couple, which determines the actual free energy of the electron transfer step, $\Delta G_{ET}^{(2)}$ (Scheme 6). In contrast, the overall free energy, $\Delta G_{AB}^{(2)}$, and the apparent equilibrium constant, $L_{AB}^{(2)}$, are determined by $E_m(Q_BH^-/Q_B^-)$ and, therefore, by pK_1, the first ionization constant of the quinol:

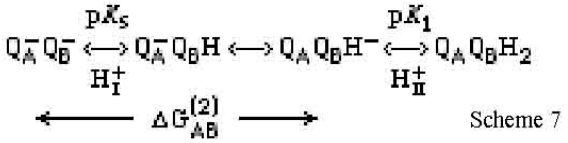

Scheme 7

The overall equilibrium of the second electron transfer is, indeed, strongly pH dependent (55). $E_m(Q_BH^-/Q_B^-)$ becomes more negative with increasing pH and approaches

and passes $E_m(Q_A^-/Q_A)$ at pH 9-9.5 (33, 55, 80). Extrapolation to pH 7 yields $\Delta G_{AB}^{(2)} = -(RT/F)ln L_{AB}^{(2)} = -$ (125 ± 20) meV. McPherson *et al.* also measured net H^+ uptake in the double reduction of Q_B and found $pK_1 = 8.5$-8.7 for the (bound) Q_BH_2 state (80). This is substantially lower than that expected for QH_2 in solution ($pK_1 \approx 13$ (138)), indicating very strong stabilization (binding) of the monoanion, Q_BH^-. Because of the low value of pK_1, the second proton uptake does not provide much driving force for electron transfer *in situ,* and at pH ≥ pK_1 release of QH_2 and associated processes such as H^+ uptake are driven by exchange with excess quinone:

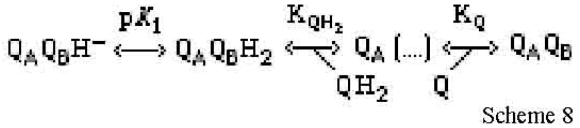

Scheme 8

Strong binding of the QH^- species is seen as slow release of quinol from RCs with the Glu^{L212}→Gln mutation, which blocks the second proton delivery, even in chromatophores where there is a great excess of quinone (139).

6.3. The ET/PT alternative

Paddock *et al.* examined several mutants with substantially impaired second electron transfer kinetics, and found that almost all still manifested the same mechanism - rapid pre-protonation to form $Q_A^-Q_BH$ followed by rate limiting electron transfer (68). The significant exception was the Asp^{L213}→Asn mutant, for which $k_{AB}^{(2)}$ is less than 1 s^{-1} at pH 7. Other mutants, however, with only slightly faster rates, still follow the same ET-limited mechanism. Thus, even for $k_{AB}^{(2)} \approx$ 1-10 s^{-1}, the rate of ET equilibration to form $Q_AQ_B^{2-}$ is still not fast compared to a slow, but very favorable, subsequent proton transfer, and it is insufficient to compete with the normal pathway *via* $Q_A^-Q_BH$. With this limit, and using the parameters $k_o = 2 \times 10^9$ s^{-1} and $\Delta G_{ET}^{(2)} = +0.24 \pm 0.03$ eV ((81), and C.A.W., in prep.), we can calculate $\lambda = 1.6 \pm 0.1$ eV for the classical Marcus equation (or 2.4 ± 0.1 eV, for the quantized form) (Eqn 3, Section 6.1). This is substantially larger than the equivalent estimate for the PT/ET route (see Sections 6.1.1 and 7.2.3), and can be readily understood as a prohibitive factor for this pathway. Combined electrostatic/molecular mechanics calculations show that the protein around the Q_B site undergoes rapid dielectric saturation as the negative charge on Q_B is increased above 1 in the computational parameters (M. R. Gunner, personal communication). This is consistent with a substantially larger λ for the 2nd ET compared to the 1st, and would also contributes to a low value for $E_m(Q_B^{2-}/Q_B^-)$,making $\Delta G_{ET}^{(2)}$ for this route quite unfavorable.

7. PROTON TRANSFER PATHWAYS

The proximal Q_B position is 13-15 Å from the aqueous phase at its closest approach, and it is inevitable that transfer of protons from the medium to Q_B, through parts of the H and L subunits, is facilitated by hydrogen bonded chains or networks. From the X-ray structure of the RC a number of putative, but incomplete, H^+ conducting pathways can be seen to converge on the Q_B site, terminating in the region of Glu^{L212} and Asp^{L213} (140). The discovery of inhibition by certain divalent, transition metal cations has now focussed attention on one of these.

Utschig *et al.* first observed that Zn^{2+} inhibited the 1st ET and bound stoichiometrically to RCs (141). They identified a possible binding site on the surface of the RC - a cluster of histidine residues in the H subunit - and suggested that the effect might arise from damping of protein motions. Subsequently, Paddock *et al.* found that the 2nd ET was similarly inhibited, and that many divalent metal ions were active with varying degrees of inhibition from 10-100 fold, and they proposed the effect was on proton entry (142). In addition to Zn^{2+}, effective metals include Cd^{2+}, Cu^{2+}, Co^{2+} and Ni^{2+}, but not Fe^{2+}, Ca^{2+}, or Mg^{2+}. The binding sites for Zn^{2+}, Cd^{2+} and Ni^{2+} were identified by crystallography (143) and found to be close to that suggested by Utschig *et al.* (see Figure 3). Zn^{2+} and Cd^{2+} were bound to His^{H126}, His^{H128} and Asp^{H124}, and Ni^{2+} was bound to His^{H126} and Asp^{M17}. Asp^{L210} is also close but is not directly bonded to either metal.

The inhibition is an essentially kinetic phenomenon and any effects on the electron transfer equilibria, for example as might be caused by the electrostatic potential at Q_B, were minor. Instead, the distinctly surface nature of the binding sites suggested that they identified a unique entry point for H^+ ions. This was confirmed by showing that the inhibited rate of the 2nd ET was not dependent on the free energy of the reaction, i.e., it was no longer rate limited by ET but, presumably, by proton transfer (142). A subsequent survey of mutations in the region between Q_B and the surface site revealed a strong synergy of the metal effects with residues Asp^{L210} and Asp^{M17}. Mutation of either one had little effect on electron and proton transfer rates, but the effect of metals was now more profound (144). Mutation of both residues together, however, caused a dramatic inhibition, with no additional metal effect (145).

Since the PT equilibrium is normally on the order of 10 times faster than ET, but when inhibited by metals, etc, is about 100 fold slower, this work identified a proton conduction pathway to the Q_B site that is at least 1000 times more effective than any alternative pathway (144). It was also shown to be active in delivering protons to the acid cluster on the first flash (especially at pH > 8.5, when Glu^{L212} is initially ionized), as well as both protons necessary for reduction of Q_B^- to quinol (146). With a single entry point, the common initial path must bifurcate to deliver protons to O1 of Q_B, *via* Glu^{L212}, and to O4, *via* Asp^{L213} and Ser^{L223}. For both cases, crystallographically resolved water molecules contribute continuity to the putative paths, which, in the inhibited, metal-bound case, are more or less complete. However, in the uninhibited state (no bound metals), the path is not so well defined and there are spans that are "missing" in the sense that there is no apparent contact for proton transfer. At these points, it is likely that the conduction pathway is dynamically assembled, either by diffusive water or, possibly, by large scale motions of residue side chains such as Asp^{L210}. In metal-bound RCs, a substantial amount of ordering was

seen for Glu^{H173}, and sidechain mobility was suggested to play a critical role in proton conduction (143).

7.1. Intraprotein proton transfer - the terminal steps

Mutagenesis studies have shown that many residues, identified as important in the charge stabilization events of the 1st electron transfer, are also critical for the delivery of protons to Q_B, accompanying the 2nd ET reduction to quinol. Notably, Glu^{L212}, Asp^{L213} and Ser^{L223} play key roles as terminal elements of the proton delivery path. The second ET has potentially conflicting requirements of the local electrostatic potential. The transfer of electrons will be assisted by a positive potential, while the delivery of protons will be aided by a negative potential. However, proton delivery, unlike electron transfer, will also be affected by the potential along the conduction path, at least insofar as it modulates the pK_a values of proton carriers. It is therefore not surprising that the responses to mutations are complex.

Mutation of either Asp^{L213} or Ser^{L223} to nonionizable residues causes almost total failure of delivery of the 1st proton, which must precede the transfer of the 2nd electron (33, 40, 147), and mutation of Glu^{L212} leads to an equally dramatic inhibition of the 2nd proton delivery, which occurs after the 2nd electron (39). However, although Glu^{L212} and Ser^{L223} are apparently conserved in all homologous bacterial sequences, Asp^{L213} is not. The critical role of Ser^{L223} is further emphasized by the fact that it, and His^{L190}, are the only residues of the bacterial Q_B binding site that are fully conserved in the homologous site of Photosystem II, in plants and cyanobacteria (148). However, unlike His^{L190}, Ser^{L223} is not involved in specific binding interactions with the oxidized quinone, in either proximal or distal Q_B positions, but it does hydrogen bond to the semiquinone. Furthermore, although Ala and Asn are non-functional substitutes for Ser^{L223}, Gly is quite functional (149). This was suggested to be due to the sequestering of a novel water molecule that could function in the place of the serine OH, implicating Ser^{L223} in a true proton transfer function. Aspartic acid is also a functional substitute (149), but attempts to modify the functional pK_a of residue L223 by mutation to cysteine resulted in a totally inactive Q_B site, possibly due to covalent crosslink formation between the quinone and the cysteine sulfhydryl (E. Takahashi and C. A. Wraight, unpublished). Crosslinking between cysteine and a methyl-substituted quinone has been proposed as a mechanism for the anticoagulation action of oxidized vitamin E , which inhibits vitamin K-dependent γ-carboxylase (150).

7.1.1. Proton delivery to O1 (carbonyl) of Q_B (H^+_I in Scheme 5)

Calculations show Ser^{L223} as a hydrogen bond donor to ionized Asp^{L213}(-) in the ground state (Q_AQ_B with Q_B proximal), but to the C1 carbonyl oxygen of Q_B^- in the $Q_AQ_B^-$ state (37). This switch-like motion sets up Ser^{L223} to deliver a proton to the O1 position of Q_B on the second turnover. In the latter configuration, the serine also accepts a hydrogen bond from $Asp^{L213}H$, so the proton transfer to Q_B^- can be very closely coupled to resupply from the carboxylic acid group. In the functional Ser^{L223}→Asp mutant, transfer of a proton from one carboxyl oxygen could also be immediately compensated by protonation of the other. On the other hand, the non-functionality of the Ser^{L223}→Asn mutation indicates that, even though the protonated amide carbonyl HN-C=OH^+ is generally less acidic than C-OH_2^+ (151), e.g., of serine, abstraction of a proton from $Asp^{L213}H$ and rotation of the protonated amide of Asn^{L223} is not a viable option.

From the X-ray structure of the *Rps. viridis* reaction center (152, 153), where the Asn^{L213}/Asp^{M44} combination prevails, it is clear that Asp^{M44} is well positioned to play the same role in this species, and can certainly engage in hydrogen bonding with Ser^{L223}. This also accounts for the high level of functionality of the Asn^{M44}→Asp second site revertant of the Asp^{L213}→Asn primary mutation in *Rba. sphaeroides*. However, other second site revertants are generally of much lower competence and do not present alternative configurations for the proton transfer role of Asp^{L213}. As noted for the 1st ET, almost all the reversion mutations can be viewed as restoring some negativity to the electrostatic potential of the region - either by adding a new acidic group, e.g., Asn^{M5}→Asp (154) and Gly^{L225}→Asp (155), or by removing a basic group, e.g., Arg^{M233} (66, 67), Arg^{L217} (154) or Arg^{H177} (68). Thus, an additional function, contributed to by Asp^{L213} and other members of the acidic cluster, may be to establish the prevailing electrostatic potential around the Q_B site, thereby setting the functional pK_a values of various groups, as well as Q_B^-, itself. A major role of this sort was ascribed to Glu^{H173} (64). In mutants lacking either Asp^{L213} or Glu^{H173}, several small inorganic ions, like azide, can restore partial or even complete function (64, 156). This was originally suggested to indicate proton-carrying activity of the weak acids of these ions, as proposed for the function of azide in "rescuing" certain bacteriorhodopsin mutants (157), but it may also be due to the anionic forms binding within the protein, thereby restoring a functionally negative potential to critical regions of the H^+ conduction pathway (64).

7.1.2. Proton delivery to O4 (carbonyl) of Q_B (H^+_{II} in Scheme 5)

To complete the formal reduction of Q_B, a second H^+ must reach the C4 carbonyl oxygen. This could come from the imidazole $N_\delta H$ of His^{L190}, which must then be reprotonated, or the Q_BH^- monoanion could disengage from its hydrogen bond with His^{L190} and be protonated directly. The pK_a for histidine, to form the imidazolate anion, is about 14 in solution. Liganding to the iron will almost certainly lower the pK_a, as it does in the Rieske iron-sulfur center of the Cyt bc_1 complex (158, 159). However, the decrease in pK_a is not large in the Fe^{2+} state (pK_a ≈ 12.5 in the Cyt bc_1 complex), and may not be enough to make His^{L190} an adequate proton donor to QH^- (pK_a ≈ 8.7 *in situ* (160)). The kinetic responses to mutation of Glu^{L212}, e.g., to glutamine or alanine, implicate this residue in the transfer of the second proton. Mutant studies show that other structural solutions support viable growth, but the kinetic competence of these revertants has not been well established. Nevertheless, it is interesting to note that compensating second-site substitutions to mutations at

Glu^{L212} overlap considerably with those for Asp^{L213} mutations (136, 161), and with the same general property of restoring acidic or removing basic groups, some of which are at a considerable distance, e.g., the guanidinium group of Arg^{M233} is 15-17Å from Q_B(proximal) and 13-14Å from Glu^{L212} and Asp^{L213}. However, the Q_A site mutation, Ala^{M247}→Tyr, which restores some activity to the Glu^{L212}→Gln mutant, is an exception to this rule (56). It seems, therefore, that Glu^{L212} is not strictly required although it is probably kinetically vastly superior. Whether restoration of significant function requires some adjustment of the electrostatic potential profile will have to await computational studies, but it must, somehow, induce proton transferring capabilities in other entities. Since no other ionizable residues come within range of the quinone headgroup, the most likely alternatives are water molecules, including "new" ones not present in the wild type structure, such as are seen in the X-ray structure of the Arg^{M233}→Cys mutation (69).

A role for water is strongly suggested by its ability to invade the Q_B site when quinone is absent or bound in the distal position (90, 91, 101, 162), and by the fact that the Glu^{L212} side chain is probably too far from the carbonyl O4 to donate directly. It is therefore likely that water is the final donor, either directly to the quinol or to reprotonate His^{L190}, and delivery of the second proton can be envisioned as being coupled to the unbinding motions of the quinol and the entry of water molecules into the site. The water channels that have been described in the RC structure are a possible hydraulic mechanism for this purpose (101, 140).

Glu^{L212} is well endowed with water contacts in all states, especially when the quinone is absent. This has prompted Mulkidjanian and coworkers to propose that Glu^{L212} has a fairly normal carboxylic pK_a ≈ 6 when the proximal position is unoccupied, due to the water molecules present, but a substantially elevated pK_a ≈ 9.5 when quinone enters, due to the formation of a hydrogen bond between -COOH and the C3'-methoxy oxygen and to the lower polarity of the pocket when the water is displaced (113). (This was discussed further in Section 5.4.4). It should be noted, however, that none of the available X-ray structures shows such a configuration for L212-Q_B(proximal).

7.2. Proton transfer kinetics

For energetically near-neutral or favorable proton transfer between hydrogen bonded components (ΔpK = $pK_{acceptor}$ - $pK_{donor} \geq 0$), the pair-wise rate can be expected to be very fast, with a maximum on the order of 10^{12} s^{-1} (163-165). However, known protein structures indicate that extensive proton transfer pathways are built on diverse functional groups, especially side chain carboxylic acids, alcohols and imidazole, and water, with solution pK_a values ranging from -2 to 7 (and even 16 for –OH/–O^-). The effect of unfavorable pK differences can be described by various free energy relationships, e.g., Brönsted, Marcus, Eigen, etc, and the experimental challenge is to vary ΔpK in a controlled manner.

Even for substantially unfavorable ΔpK steps, the proton transfer rate need not be limiting for a coupled reaction. This is likely the case in the native RC pathway, where electron transfer is quite robust towards mutational modifications that have significant effects on equilibrium protonation parameters. A few noteworthy exceptions identify the key residues Glu^{L212}, Asp^{L213}, Ser^{L223}, Glu^{H173}, Asp^{L210}, Asp^{M17} and His^{H126} and His^{H128}. However, even amongst these, only a small subset gives rise to clear onset of rate limitation by proton transfer, i.e., where PT has become slow relative either to the conformational change that normally controls the 1st electron transfer, or to ET itself in the 2nd electron transfer. These include non-ionizable substitutions at Asp^{L213} (68), the double mutation of Asp^{L210} and Asp^{M17} (145), and the double mutation of the two surface histidine residues, His^{H126} and His^{H128} (2xHis mutant) (105). The latter identifies a unique entry site for protons into the conduction pathway to the Q_B site, and the pick-up point from the surface/bulk interphase.

At pH > 8 in the 2xHis mutant, proton transfer from the surface to the internal proton conduction path is rate limiting for both the 1st and the 2nd electron transfer (146). Donation by water (as H_3O^+) is evidently ineffective because, although the intrinsic rate constant is very high (approx. 10^{11} M^{-1} s^{-1}), the concentration is too low. However, it may become sufficient at lower pH, as the electron transfer rate in this mutant approaches that of wild type at pH 7 (105). In contrast, the native His configuration appears to provide a surface source of high effective concentration and adequate acidity over the entire pH range. This function can be restored by soluble cationic buffers that bind weakly and "rescue" the mutant (105, 166).

7.2.1. Proton transfer coupled to the first electron

Paddock *et al.* (166) have used the buffer rescue approach with 2xHis mutant RCs to explore the initial steps of proton transfer in the 1st electron transfer reaction. At low concentrations of buffer, the recovered rates of electron transfer yielded second-order rate constants that were a function of the pK_a of the rescuing buffer. A very recognizable Brönsted plot (log k *vs*. pK_a) was obtained, with a slope of -1 at pH values above an apparent pK_a ≈ 4. The behavior was accounted for by the following (abbreviated) model for the 1st electron transfer, with imidazole (Im) as the rescuing buffer most similar to the native histidine:

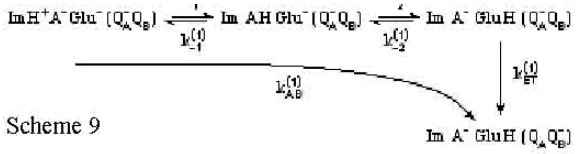

Scheme 9

Glu represents the terminal acceptors, e.g., the acid cluster, "Glu^{L212}", with an apparent pK_a > 8.5. However, the analysis showed the necessary involvement of a much more acidic intermediate, A^-/AH, with pK_a ≈ 4-5, consistent with a typical carboxylic acid. For imidazole as initial donor, the effective pK_a at the surface was estimated to be ≈10, making the initial PT considerably uphill. Independent data suggest that at least one functional pK_a at the intact

(non-mutant) entrance site is more like 7 (167), perhaps because of mutual interactions between the two histidines.

With the equilibrium parameters for imidazole, it was possible to estimate the individual rate constants to be:

$$k_1^{(1)} \approx 10^6\ s^{-1}; \qquad k_{-1}^{(1)} \approx 10^{11}\ s^{-1}; \qquad k_2^{(1)} \approx 10^{10}\ s^{-1}$$

with an order of magnitude accuracy. $k_{-2}^{(1)}$ depends on the pK_a of the terminal acceptor, which is uncertain. However, for pK_a(Glu^{L212}) ≈ 8.5, $k_{-2}^{(1)}$ would be about $10^7\ s^{-1}$.

The overall rate constant for proton transfer to the terminal acceptor is given by:

$$k_{H+}^{(1)} = k_1^{(1)} k_2^{(1)} / (k_{-1}^{(1)} + k_2^{(1)}) \qquad \text{Eqn. 5}$$

and was estimated at $10^5\ s^{-1}$, within a factor of 2 (166). For the native histidine configuration, with a functional pK_a of about 8, the overall rate will change, but not markedly. Thus, the internal rate constants constitute equilibration rates ($k_1^{(1)} + k_{-1}^{(1)}$, $k_2^{(1)} + k_{-2}^{(1)}$, etc) that are certainly fast compared to the observed reaction, $k_{AB}^{(1)}$. However, the reaction is also not rate limited by electron transfer (see Section 5.4).

Representation of the terminal acceptor in Scheme 9 as "Glu^{L212}" is a pure formality, but it is somewhat misleading. For example, Glu^{L212}, itself, is unlikely to be in contact with whatever residue is represented by A. The proton conduction path from the surface to any candidate targets of the acid cluster, or to Q_B is almost complete in some structures, notably those with bound metals at the histidine cluster (PDB files 1ds8, 1dv3 and 1dv6). However, the absence of complete connectivity in any uninhibited structures may indicate a more dynamic nature of the functional pathway, involving movement of waters and, possibly, sidechains, for example of Asp^{L210}. Most of the water molecules required to bridge between amino acid side chains can be seen in various different X-ray structures.

The general picture appears to be similar to the situation seen in carbonic anhydrase, where a functional chain of 3-5 water molecules is involved (168, 169). Both mutant studies (169-171) and molecular dynamic simulations (172-174) of carbonic anhydrase indicate that the active configuration of the water chain is dynamically assembled. This defines the proton path in carbonic anhydrase as a dynamic entity, as also proposed for superoxide dismutase (175), and actually visualized in bacteriorhodopsin (11, 176). A highly dynamic role has also been proposed for water in both conduction and gating of proton translocation in the proton pumping heme-copper oxidases (177).

Since the pK_a of water (approx. -2, on a molar basis) is quite extreme compared to other groups in the chain of events, it might be expected that the rate limiting step in a water-containing path would be one that involves proton transfer to or from water. However, in carbonic anhydrase, a rather successful Marcus analysis of the kinetics yields a description based simply on the relatively small pK_a difference between terminal acceptors and donors. The only apparent contribution from water is in the work terms of the formal rate expression, interpreted as the cost of assembling the fully hydrogen bonded pathway (171, 178). Such a contribution is reasonable, but it is not obvious why proton transfer to or from water is not more evident. It implies that substantial pK_a shifts exist for any water that is directly connected to an acceptor or donor. Such shifts - i.e., the local electrostatic environment - are evident in molecular dynamics and quantum chemical simulations of proton transfer (179-181).

At the present time the resolution of the X-ray structures is insufficient to allow unequivocal placement of water molecules in RCs, although there are a number of consensus positions identified (Figure 7). The apparent need for bridges of no more than 1 or 2 water molecules in the putative pathway may simplify the process of pathway activation and minimize this component of the energetic barrier. This may partially account for why net transfer (proton equilibration) is so fast over a distance of 14 Å, nearly twice the length of that seen in carbonic anhydrase.

7.2.2. Proton transfer coupled to the second electron

In the 2xHis mutant, the 2nd ET is rate limited by proton transfer similarly to the 1st ET, but the overall rate constant (and hence k_{H+}) is approx. 5 times slower (166). This was suggested to reflect the different pK_a values of the terminal acceptor - approx. 4.5 for Q_B^- *vs.* 8.5 for "Glu^{L212}". However, as just discussed, Scheme 9 and its equivalent for the 2nd ET do not properly identify the terminal acceptor species. The 5-fold difference in protonation rate for the 2nd ET more likely reflects equivalent changes in k_1 or k_2, due to relatively small shifts in the pK_a of A or other intermediates, induced by the charge on Q_B^-. The internal proton transfer rate constants are therefore not very different for the 1st and 2nd ET events, and the proton equilibration rates are clearly adequate to satisfy the required inequality for non-rate limiting proton transfer in the wild type ($k_{eq} > 10^6\ s^{-1}$).

At the present time, little is known about the kinetics of the second proton (H_{II}^+) delivered to Q_BH^-. The relative pK_a values for the ultimate donor (Glu^{L212}H, pK_a ≈9, or His^{L190}, pK_a ≈ 12) and acceptor (Q_BH^-, pK_a ≈ 8.5) are either quite well matched (Glu^{L212}H) or not very unfavorable (His^{L190}) for transfer. Thus, the proton transfer step should be intrinsically fast and rate limitation is likely to reside in conformational movements of the quinol or of water molecules necessary to bridge the gap. At room temperature, in wild type RCs, H_{II}^+ is transferred sufficiently rapidly that it cannot be resolved from the first proton. However, in chromatophores, at temperatures below 15 °C, it becomes distinguishable and it clearly has a substantially higher activation energy than the electron transfer-limited first proton (182). The authors suggested that this arises from the energy needed to undock the quinol monoanion from its hydrogen bond with His^{L190}, although

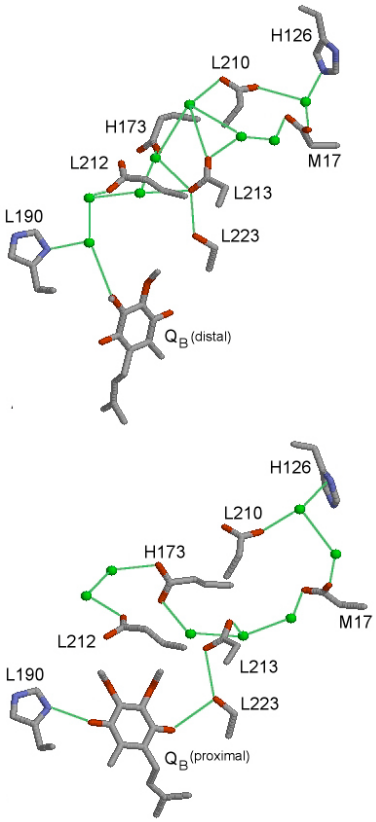

Figure 7. Consensus water positions in the Q_B protonation pathway. Top: the "dark state", with Q_B in the distal position (PDB files: 1prc, 1aij, 1ds8, 1dv6). Bottom: the "light state", with Q_B in the proximal position (PDB files: 1aig, 1dv3, 1qov). The latter file (1qov) is for a mutant lacking Q_A and is not a light activated structure, but was included because Q_B is in the proximal positon. Not all waters shown are in any single structure file, but significant overlap exists between different structures.

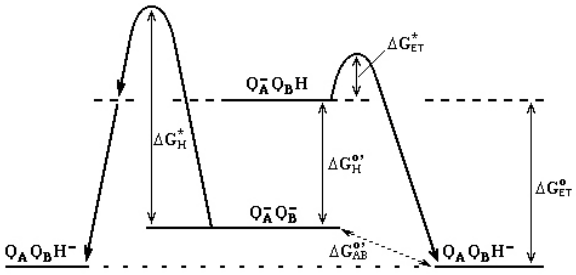

Figure 8. Activation diagram for the second electron transfer. Right side: ET-limited mechanism, as in wild type and many mutant RCs. Left side: PT-limited (or non-ET-limited) mechanism, as in wild type RCs plus divalent transition metal ions (Ni^{2+}, Cd^{2+}, Zn^{2+}, etc), and certain mutants, notably L213DN, L210DN/M17DN, and H126HA/H128HA (2xHis).

it could also be due to removing the fully protonated quinol from an imidazolate His^{L190}.

7.2.3. Temperature dependence of the coupled electron and proton transfers

Temperature dependence measurements present an alternative approach to the free energy relationships obtained by the buffer rescue method of Paddock *et al.* (166) described above (Section 7.2.1), and the two are complementary in developing proper understanding of mechanism - for example, to separate the influences of activation energetics and adiabaticity. According to the working model for coupled electron-proton transfer on the second turnover (Scheme 6), the activation parameters for wild type RCs (ET-limited) must include the uphill protonation pre-equilibrium and an activation free energy term for the electron transfer, i.e., $\Delta G_T^* = \Delta G_H^o + \Delta G_{ET}^*$. This is shown on the right side of Figure 8. EPR data on the $Q_A^- Q_B^-$ state (119, 120) provide the necessary electronic coupling data for the preexponential factor (k_o = 3 x 10^9 s^{-1}) in a Marcus-type description of the ET step (Eqn. 3). This allows one to obtain the total (or apparent) activation parameters, ΔH_T^* and ΔS_T^* and, hence, ΔG_T^*, from the T-dependence. From this, the expected contribution of the protonation equilibrium, i.e., ΔG_H^o = 2.3RT(pH–pK_a), yields $\Delta G_{ET}^* \approx 0.21$ eV, at pH 7.5 (C. A. Wraight and P. Maróti, unpublished). With a reasonable estimate for the driving force for the electron transfer step (ΔG_{ET}^o = -0.25 eV (45, 81, 117)), this result predicts a value for the reorganization energy, $\lambda \approx 1.3$ eV. This agrees well with previous estimates (125-127, 183) (see Section 6.1.1), indicating that this analysis is appropriate for the native, ET-limited reaction path.

The component enthalpy and entropy contributions to the activation free energy can also be obtained with reasonable assumptions about the thermodynamics of the proton equilibrium. There is a vast literature on the thermodynamics of ionization equilibria, which shows a good linear correlation between standard enthalpy and entropy for "normal" (oxygen and nitrogen) acids and bases, including semiquinones and hydroquinones (184-186). For p$K_a \approx 4.5$, as for Q_B^-, these data indicate $\Delta H_H^o \approx$ -6 kcal/mol and $T\Delta S_H^o \approx$ +4 kcal/mol, for proton association. However, even without knowledge of the absolute values of ΔH_H^o and ΔS_H^o, it is clear that the pH dependence of the activation entropy should reflect the negative entropy of mixing for the protonation equilibrium, $d\Delta S_T^*/dpH \approx d\Delta S_H^{o'}/dpH < 0$. For wild type RCs (ET-limited), this is observed (C.A. Wraight and P. Maróti, unpublished) - the slope is less than that expected from –2.3R(pH–pK_a), but this is readily accommodated by a pH-dependent pK_a value, due to the changing electrostatics in the protein as residues ionize (see Section 6.1.2) (26, 81). Thus, it seems reasonable to conclude that the true activation process (ΔS_{ET}^*) does not have a significant pH dependence.

For non-ET limited cases (left side of Figure 8), the analysis is necessarily different and the normal approach, following the chemical field, would be to apply transition state theory with a transmission coefficient (κ) of 1. Consideration of any degree of non-adiabaticity would be necessary to obtain absolute values of the enthalpy and entropy of activation, but the pH dependence of these

parameters is not dependent on the value of κ (except that it be pH independent). It is clear, for example, that if the transition state involves proton uptake, the pH dependence of the activation entropy should appear as a negative entropy of mixing, as described above. In fact, almost any manipulation that alters the rate limitation - by mutation (but not including the singular mutant L213DN, Asp^{L213}–›Asn) or by binding of divalent cations like Cd^{2+} or Ni^{2+}, which inhibit the capture and entry of H^+ into the proton conducting pathway (142) - results in an apparent (total) activation entropy, ΔS_T^*, that exhibits a substantially *positive* pH dependence (C.A. Wraight and P. Maróti, unpublished). It is unlikely that the ET step is intrinsically altered by these mutations or by metal binding, which are all at some distance from the quinone sites. Thus, the pH dependence corresponds to whatever non-ET event modifies the observed rate, e.g., the rapid protonation pre-equilibrium (in the ET-limited case), or a rate limiting proton transfer (PT-limited).

Thus, modification of the proton pathway in a variety of ways reveals a proton conduction mechanism with a positive pH dependence for the activation entropy. This strongly suggests that H^+ binding, *per se,* is not involved in the rate limiting step. An attractive alternative is the formation of a hydrogen bonded pathway, possibly including solvent water, as has been proposed for carbonic anhydrase (187, 188) and superoxide dismutase (175), and almost visualized in bacteriorhodopsin (11, 176). Conceivably the positive pH dependence reflects an increasing surface charge on the protein and its influence on counter-ion binding/release that accompanies the bonding rearrangements involved in establishing the proton conduction pathway.

The distinct behavior of the L213DN mutant is striking and indicates a very different kind of limitation, including the likelihood of significant non-adiabaticity. The negative pH dependence of ΔS_T^* in this mutant may indicate a role for H^+ uptake in reaching the activated state for PT.

7.3. Proton supply

H^+ ions enter the proton conduction pathway at a unique site that is defined by the surface histidine/aspartic acid complex. In turn, the supply of protons from the bulk phase can occur by multiple, parallel pathways. These include (i) bulk (aqueous) H^+-ion diffusion, (ii) protolysis of water, and (iii) transfer from a diffusible donor, e.g., buffer.

Eqns. 6

i. $RC^* + H_3O^+ \underset{k_A}{\overset{k_H}{\rightleftharpoons}} RCH^+ + H_2O$

ii. $RC^* + H_2O \underset{k_{OH}}{\overset{k_B}{\rightleftharpoons}} RCH^+ + OH^-$

iii. $RC^* + DH \underset{k_{-D}}{\overset{k_D}{\leftrightharpoons}} RCH^+ + D^-$

The combination of these is generally expected to give very fast bulk transfer rates (130, 189). However, for proton binding by the $P^+Q_A^-$ state at alkaline pH, the rate of H^+ uptake detected in the bulk phase, although fast, was slower than expected and a limitation was proposed to reside in protein conformational equilibria or dynamics (26). In chromatophores, net H^+ uptake is similarly retarded compared to the development of an electric potential due to internal charge transfer (which is presumed to comprise H^+ movements) (190). This indicates a rate limitation in the transfer of H^+ across the membrane interface, which was suggested to occur by protolysis of water (Reaction ii, above). This, in turn, implies a restriction on the diffusive approach of soluble buffers, which would otherwise be expected to dominate *via* Reaction iii. This description has been given some support by atomic force microscopy measurements that indicate a very low dielectric constant for water at charged surfaces, and extending some distance (1-5 nm) into the aqueous phase (191). A theoretical application of this to biological surfaces suggests that a substantial barrier exists to any ion movement normal to the surface, due to an enhanced Born energy penalty in the low dielectric of ordered water near the surface (192). This proposal, if correct, has important implications for (chemiosmotic) energy transduction in biological membrane systems, and may also be significant for the more local considerations of large, isolated proteins.

In spite of the low concentration of protons in aqueous solution at physiological pH values, the pathways for proton delivery from the bulk phase could be marginally adequate at neutral pH, without special devices. However, two additional, but related, mechanisms have been suggested to overcome any possible limitation to proton supply, both involving similar surface features of the protein - proton antennas and effective, local concentrations.

Certain configurations of ionizable surface groups, especially carboxylic acids, have been proposed to act as proton antennas, effectively harvesting H^+ from solution and transfering them on the surface by pairwise transfers (189, 193, 194). The close proximity of functional groups allows pairwise proton transfer rates on the order of 10^{12} s^{-1} (163-165) and surface hopping is considered to be made more efficient by the tendency for the dissociated H^+ to remain trapped within the Coulomb and solvent cage of the ionized carboxylate anion. At low or moderate ionic strength this could lead to long distance surface conduction, making a negatively charged system an effective antenna. Stuchebrukhov and coworkers have considered this from a somewhat different perspective (195), and conclude that the main aspect of antenna function is fulfilled simply by the known reduction of dimensionality that occurs at a plane surface (196) and is largely independent of specialized features, including charge. However, the necessary size for such an antenna to be significant was found to be substantially larger than that of a typical protein. Nevertheless, an extensive membrane surface (generally negatively charged) may well contribute in this manner.

Experimental evidence for structural enhancements of proton transport kinetics have been described for several proteins. Using fast pH jumps from laser-activated photoacids and bases, Gutman and

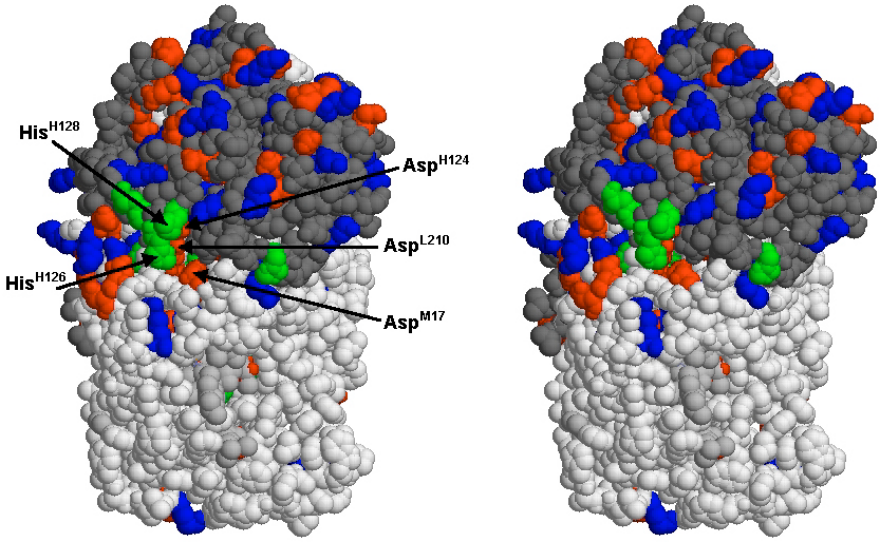

Figure 9. Ionizable residues of the *Rba. sphaeroides* reaction center (cross-eyed stereoview). The view is looking down, obliquely, at the Q_B domain, on the cytoplasmic side. The H subunit is shown in dark gray, and residues are colored as follows: acidic - red, basic - blue, histidine - green. Cofactors are in CPK coloring and some ($Bchl_B$, $Bphe_B$ and spheroidene) are visible in the bottom half of the figure. The labeled residues surround the presumed proton entrance site, and are known to be involved in proton entry and transfer. The structure file used was 1m3x.pdb.

coworkers have shown that transient residence and collection of protons does occur on discrete subsets of carboxylic acids near indicator groups covalently tethered to the surfaces of proteins, including bacteriorhodopsin (bR) (194, 197, 198), cytochrome c oxidase (199) and quinol oxidase (194). In the case of bR and quinol oxidase, the tether location was near the proton entry site. However, in bR, mutation of surface carboxylic acid residues (i.e., other than those involved in the internal conduction pathways) had no, or very little, effect on photocycle kinetics or net turnover (200). Nevertheless, long range surface transport can be seen is bR purple membranes (201-203), but this could be facilitated by the various negatively charged lipids of the purple membrane.

Further compromising the notion of a predominantly antenna contribution of the protein surface, the specific amino acid configurations that have been identified as having a significant impact on proton transfer/delivery function are dominated by histidines, for which the Coulomb cage effect is absent (although the much weaker solvent cage will remain). For histidines, however, with higher pK_a values than carboxylic acids, enhancement of proton supply can arise from an effective local proton concentration in the form of fixed buffer (189). In RCs, for example, the Q_AQ_B electron transfers in the 2xHis mutant become proton limited above about pH 8 (105), whereas the wild type is not proton limited even at pH > 10. This indicates that His^{H126} and His^{H128}, with pK_a ≈ 7 (167), are effective as local proton donors, even when less than 0.1% protonated. Furthermore, the presence of multiple groups (e.g., histidines), as is generally observed in such domains, raises the effective pK_a of the cluster - at high pH (low protonation probability) the single proton occupancy of three independent groups is upto 12 times that of a single group.

In some cases, both these enhancement mechanisms may prevail. In RCs, the key histidines are part of the surface ionic landscape that is net negative, and an antenna function of the carboxylates could be coupled to the histidines at the proton entry site. However, the distribution of charges does not obviously support this. Negatively charged surface residues are not in excess near the proton entry site of His^{H126} and His^{H128} and, with the exception of Asp^{M17}, all are roughly paired with basic residues, and many are in clear salt bridge associations (Figure 9). Asp^{L210} and Asp^{H124} are largely occluded by the histidines, and the former, at least, is implicated in the proton pathway (see above). A very similar arrangement is found in the proton-pumping heme-copper oxidases (cytochrome c oxidase (204-206) and quinol oxidase (207)), where the key residue of the D-channel, Asp^{I-132} (residue 132 of subunit I, in *Rba. sphaeroides*), is similarly placed beneath the two histidines of the proton entrance domain. However, the defined role of Asp^{I-132} is as an active component in the proton conduction pathway (9, 208), akin to that of Asp^{L210} and Asp^{M17} in RCs, and as yet there is no clear evidence that an antenna function significantly enhances net proton throughput. Conceivably, however, the submerged carboxylates of the RC (e.g., Asp^{L210}, and possibly Asp^{H124}) and oxidase (Asp^{I-132}) project a negative potential into the solvent, in much the same way as the active site of certain enzymes enhances the encounter with substrates by "electrostatic focussing", e.g., superoxide dismutase with O_2^- (209) and acetyl cholinesterase with acetyl choline (210).

8. CONCLUSIONS

The underlying concepts governing non-adiabatic electron transfer in biological processes are now quite well understood, and both theory and computation are proving

useful in describing events in photosynthetic and respiratory complexes. Proton transfer, on the other hand, which is almost certainly purely adiabatic in bioenergetic systems, requires much more structural and dynamic detail to define it kinetically. From experimental studies, the nature of the main equilibrium macrostates of the reaction center is becoming known. However, these comprise a significant number of strongly interacting microstates, and the protonation responses of the protein to new charges, such as Q_A^- and Q_B^- in reaction centers, are quite widely distributed. The essentially electrostatic nature of proton transfer reactions allows computational approaches to describing the complex equilibria involved, but these have not yet reached consensus. This may be partly due to limitations in current methodologies, but equally important is the limiting resolution of available structures and the limited use of dynamics. At the present time there are still few, direct experimental methods to probe the protonation states of the protein, with FTIR the main contributor. Nevertheless, in spite of such difficulties, the combination of computational and experimental approaches has yielded a good outline of the coupled proton-electron transfer events in the acceptor quinones of the photosynthetic reaction center of *Rhodobacter sphaeroides*, as representative of the purple non-sulfur bacteria.

9. ACKNOWLEDGEMENTS

I am grateful to Marilyn Gunner (City College of New York) for many edifying discussions. Any original work reported here was carried out with funding from the National Science Foundation (MCB99-05672).

10. REFERENCES

1. Crofts, A. R., and Wraight, C. A. The Electrochemical Domain of Photosynthesis. *Biochim. Biophys. Acta* 726, 149-185 (1983)

2. Cramer, W. A., and Knaff, D. B. Energy Transduction in Biological Membranes: A Textbook of Bioenergetics, Springer-Verlag, New York (1990)

3. Moser, C. C., Page, C. C., Cogdell, R. J., Barber, J., Wraight, C. A., and Dutton, P. L. Length, Time and Energy Scales of Photosystems. *Advances in Protein Chemistry* 63, 71-109 (2003)

4. Wraight, C. A. The involvement of stable semiquinones in the two-electron gates of plant and bacterial photosystems. In: Function of quinones in energy conserving systems. Trumpower, B. L., Ed., Academic Press, New York pp 181-197 (1982)

5. Deisenhofer, J., Epp, O., Miki, K., Huber, R., and Michel, H. X-ray structure analysis of a membrane protein complex: Electron density map at 3 Angstroms resolution and a model of the chromophores of the photosynthetic reaction center from *Rhodopseudomonas viridis*. *J. Mol. Biol.* 385, 385 (1984)

6. Deisenhofer, J., Epp, O., Miki, R., Huber, R., and Michel, H. Structure of the protein subunits in the photosynthetic reaction center of *Rhodopseudomonas viridis* at 3 Å resolution. *Nature* 318, 618-624 (1985)

7. Farid, R. S., Moser, C. C., and Dutton, P. L. Electron Transfer in Proteins. *Curr. Opin. Struct. Biol.* 3, 225-233 (1993)

8. Okamura, M. Y., Paddock, M. L., Graige, M. S., and Feher, G. Proton and Electron Transfer in Bacterial Reaction Centers. *Biochim. Biophys. Acta* 1458, 148-163 (2000)

9. Gennis, R. B. Multiple Proton-conducting Pathways in Cytochrome Oxidase and a Proposed Role for the Active-site Tyrosine. *Biochim. Biophys. Acta* 1365, 241-248 (1998)

10. Wikström, M. Proton Translocation by the Respiratory Haem-copper Oxidases. *Biochim. Biophys. Acta* 1365, 185-192 (1998)

11. Lanyi, J. K. Crystallographic studies of the conformational changes that drive directional transmembrane ion movement in bacteriorhodopsin. *Biochim. Biophys. Acta* 1459, 339-345 (2000)

12. Deisenhofer, J., and Norris, J. R. The Photosynthetic Reaction Center, Vol. I and II, Academic Press, San Diego (1993)

13. Lancaster, C. R. D., Ermler, U., and Michel, H. The structures of photosynthetic reaction centers from purple bacteria as revealed by X-ray crystallography. In: Anoxygenic Photosynthetic Bacteria. Blankenship, R. E., Madigan, M. T., and Bauer, C. E., Eds., Kluwer Academic Publishers, Dordrecht pp 503-526 (1995)

14. Kirmaier, C., and Holten, D. An assessment of the mechanism of initial electron transfer in bacterial reaction centers. *Biochemistry* 30, 609-613 (1991)

15. Zinth, W., and Kaiser, W. Time-resolved spectroscopy of the primary electron transfer in reaction centers of *Rhodobacter sphaeroides* and *Rhodopseudomonas viridis*. In: The Photosynthetic Reaction Center. Deisenhofer, J., and Norris, J. R., Eds., Academic Press, San Diego pp 71-88 (1993)

16. Woodbury, N. W., and Allen, J. P. The pathway, kinetics and thermodynamics of electron transfer in wild type and mutant reaction centers of purple nonsulfur bacteria. In: Anoxygenic Photosynthetic Bacteria. Blankenship, R. E., Madigan, M. T., and Bauer, C. E., Eds., Kluwer Academic Publishers, Dordrecht pp 527-557 (1995)

17. Maróti, P., and Wraight, C. A. Flash-induced H+ binding by bacterial photosynthetic reaction centers: comparison of spectrophotometric and conductimetric methods. *Biochim. Biophys. Acta* 934, 314-328 (1988)

18. Maróti, P., and Wraight, C. A. Flash-induced H^+ Binding by Bacterial Reaction Centers: Influences of the

Redox States of the Acceptor Quinones and Primary Donor. *Biochim. Biophys. Acta* 934, 329-347 (1988)

19. McPherson, P. H., Okamura, M. Y., and Feher, G. Light-induced proton uptake by photosynthetic reaction centers from *Rhodobacter sphaeroides* R-26. I. Protonation of the one-electron states $D^+Q_A^-$, DQ_A^-, $D^+Q_AQ_B^-$, and $DQ_AQ_B^-$. *Biochim. Biophys. Acta* 934, 348-368 (1988)

20. Shinkarev, V. P., and Wraight, C. A. Electron and Proton Transfer in the Acceptor Quinone Complex of Reaction Centers of Phototrophic Bacteria. In: The Photosynthetic Reaction Center. Deisenhofer, J., and Norris, J. R., Eds., Academic Press, San Diego pp 193-255 (1993)

21. Okamura, M. Y., and Feher, G. Proton-Coupled Electron Transfer Reactions of Q_B in Reaction Centers from Photosynthetic Bacteria. In: Advances in Photosynthesis. Blankenship, R., Madigan, M., and Bauer, C., Eds., Kluwer Academic Publishers pp 577-593 (1995)

22. Woodbury, N. W. T., and Parson, W. W. Nanosecond fluorescence from isolated photosynthetic reaction centers from *Rhodopseudomonas sphaeroides*. *Biochim. Biophys. Acta* 767, 345-361 (1984)

23. Kirmaier, C., Holten, D., and Parson, W. W. Temperature and detection-wavelenth dependence of the picosecond electron transfer kinetics measured in *Rhodopseudomonas sphaeroides* reaction centers. Resolution of new spectral and kinetic components in the primary charge separation process. *Biochim. Biophys. Acta* 810, 33-48 (1985)

24. Kirmaier, C., and Holten, D. Evidence that a distribution of bacterial reaction centers underlies the temperature and detection-wavelength dependence of the rates of the primary electron-transfer reactions. *Proc. Natl. Acad. Sci. USA* 87, 3552-3556 (1990)

25. McMahon, B. H., Müller, J. D., Wraight, C. A., and Nienhaus, G. U. Electron transfer and protein dynamics in the photosynthetic reaction center. *Biophys. J.* 74, 2567-87 (1998)

26. Maróti, P., and Wraight, C. A. Kinetics of H^+ Ion Binding by the $P^+Q_A^-$ State of Bacterial Photosynthetic Reaction Centers: Rate Limitation within the Protein. *Biophysical Journal* 73, 367-381 (1997)

27. Wyman, J., and Gill, S. J. Binding and Linkage: Functional Chemistry of Biological Macromolecules, University Science Boks, Mill Valley, CA (1990)

28. Kirkwood, J. G. Theory of solutions of molecules containing widely separated charges with special application to zwitterions. *J. Chem. Phys.* 2, 351-361 (1934)

29. Warshel, A., and Russell, S. T. Calculations of electrostatic interactions in biological systems and in solutions. *Q. Rev. Biophys.* 17, 283-422 (1984)

30. Gilson, M. K., and Honig, B. Energetics of charge-charge interactions in proteins. *Proteins* 3, 32-52 (1988)

31. Honig, B., and Nicholls, A. Classical electrostatics in biology and chemistry. *Science* 268, 1144-1149 (1995)

32. Baciou, L., Sinning, I., and Sebban, P. Study of Q_B^- Stabilization in Herbicide-Resistant Mutants from the Purple Bacterium *Rhodopseudomonas viridis*. *Biochemistry* 30, 9110-9116 (1991)

33. Takahashi, E., and Wraight, C. A. Proton and Electron Transfer in the Acceptor Quinone Complex of *Rhodobacter sphaeroides* Reaction Centers: Characterization of Site-directed Mutants of the Two Ionizable Residues, Glu^{L212} and Asp^{L213}, in the Q_B-binding Site. *Biochemistry* 31, 855-866 (1992)

34. Sebban, P., Maróti, P., Schiffer, M., and Hanson, D. K. Electrostatic dominoes: Long distance propagation of mutational effects in photosynthetic reaction centers of *Rhodobacter capsulatus*. *Biochemistry* 34, 8390-8397 (1995)

35. Cherapanov, D. A., Bibikov, S. I., Bibikova, M. V., Bloch, D. A., Drachev, L. A., Bloch, D. A., Gopta, O. A., Oesterhelt, D., Semenov, A. Y., and Mulkidjanian, A. Y. Reduction and protonation of the secondary quinone acceptor of *Rhodobacter sphaeroides* photosynthetic reaction center: Kinetic model based on a comparison of wild-type chromatophores with mutants carrying Arg–›Ile substitution at sites 207 and 217 in the L-subunit. *Biochim. Biophys. Acta* 1459, 10-34 (2000)

36. Shinkarev, V. P., Takahashi, E., and Wraight, C. A. Electrostatic Interactions and Flash-Induced Proton Uptake in Reaction Centers from *Rb. sphaeroides*. In: The Photosynthetic Bacterial Reaction Center II: Structure, Spectroscopy and Dynamics. Breton, J., and Verméglio, A., Eds., Plenum Press, New York pp 375-387 (1992)

37. Alexov, E., and Gunner, M. R. Calculated protein and proton motions coupled to electron transfer: Electron transfer from Q_A^- to Q_B in bacterial photosynthetic reaction centers. *Biochemistry* 38, 8254-8270 (1999)

38. Taly, A., Sebban, P., Smith, J. C., and Ullmann, G. M. The position of Q_B in the photosynthetic reaction center depends on pH: A theoretical analysis of the proton uptake upon Q_B reduction. *Biophys. J.* 84, 2090-2098. (2003)

39. Paddock, M. L., Rongey, S. H., Feher, G., and Okamura, M. Y. Pathway of proton transfer in bacterial reaction centers: Replacement of glutamic acid 212 in the L subunit by glutamine inhibits quinone (secondary acceptor) turnover. *Proc. Natl. Acad. Sci. USA* 86, 6602-6606 (1989)

40. Takahashi, E., and Wraight, C. A. A Crucial Role for Asp^{L213} in the Proton Transfer Pathway to the Secondary Quinone of Reaction Centers from *Rhodobacter sphaeroides*. *Biochim. Biophys. Acta* 1020, 107-111 (1990)

41. Gunner, M. R., and Honig, B. Calculations of proton uptake in *Rhodobacter sphaeroides* reaction centers. In: The Photosynthetic Bacterial Reaction Center: Structure, Spectroscopy and Dynamics II. Breton, J., and Verméglio, A., Eds., Plenum, New York pp 403-410 (1992)

42. Beroza, P., Fredkin, D. R., Okamura, M. Y., and Feher, R. Electrostatic calculations of amino acid titration electron transfer, $Q^-_AQ_B$---> $Q_AQ_B^-$, in the reaction center. *Biophys. J.* 68, 2233-2250 (1995)

43. Lancaster, C. R. D., Michel, H., Honig, B., and Gunner, M. R. Calculated Coupling of Electron and Proton Transfer in the Photosynthetic Reaction Center of *Rhodopseudomonas viridis*. *Biophys. J.* 70, 2469-2492 (1996)

44. Alexov, E. G., and Gunner, M. R. Incorporating Protein Conformational Flexibility into the Calculation of pH-dependent Protein Properties. *Biophys. J.* 74, 2075-2093 (1997)

45. Paddock, M. L., Rongey, S. H., McPherson, P. H., Juth, A., Feher, G., and Okamura, M. Y. Pathway of Proton Transfer in Bacterial Reaction Centers: Role of Aspartate-L213 in Proton Transfers Associated with Reduction of Quinone to Dihydroquinone. *Biochemistry* 33, 734-745 (1994)

46. Hanson, D. K., Nance, S. L., and Schiffer, M. Second site mutation at M43 (Asn–›Asp) compensates for the loss of two acidic residues in the $Q_B$site of the reaction center. *Photosynth. Res.* 32, 147-153 (1992)

47. Michel, H., Weyer, K. A., Gruenberg, H., Sunger, I., Oesterhelt, D., and Lottspeich, F. The 'light' and 'medium' subunits of the photosynthetic reaction centre from *Rhodopseudomonas viridis*: isolation of the genes, nucleotide and amino acid sequence. *EMBO J.* 5, 1149-1158 (1986)

48. Belanger, G., Bernard, J., Corriveau, P., and Gingras, G. The structural genes coding for the L and M subunits of *Rhodopirillum rubrum* photoreaction center. *J. Biol. Chem.* 263, 7632-7638 (1988)

49. Ovchinnikov, Y. A., Abdulaev, N. G., Zolotarev, A. S., Shmukler, B. E., Zargarov, A. A., Kutuzov, M. A., Telezhinskaya, I. N., and Levina, N. B. Photosynthetic reaction centre of *Chloroflexus aurantiacus*..I. Primary structure of L-subunit. *FEBS Lett.* 231, 237-242 (1988)

50. Ovchinnikov, Y. A., Abdulaev, N. G., Zolotarev, A. S., Shmukler, B. E., Zargarov, A. A., Kutuzov, M. A., Telezhinskaya, I. N., and Levina, N. B. Photosynthetic reaction centre of *Chloroflexus aurantiacus.* II. Primary structure of M-subunit. *FEBS Lett.* 232, 364-368 (1988)

51. Hienerwadel, R., Grzybek, S., Fogel, C., Kreutz, W., Okamura, M. Y., Paddock, M. L., Breton, J., Nabedryk, E., and Mäntele, W. Protonation of Glu L212 following Q_B^- Formation in the Photosynthetic Reaction Center of *Rhodobacter sphaeroides*: Evidence from Time-resolved Infrared Spectroscopy. *Biochemistry* 34, 2832-2843 (1995)

52. Nabedryk, E., Breton, J., Hienerwadel, R., Fogel, C., Mäntele, W., Paddock, M. L., and Okamura, M. Y. Fourier Transform Infrared Difference Spectroscopy of Secondary Quinone Acceptor Photoreduction in Proton Transfer Mutants of *Rhodobacter sphaeroides*. *Biochemistry* 34, 14722-14732 (1995)

53. Nabedryk, E., Breton, J., Okamura, M. Y., and Paddock, M. L. Proton uptake by carboxylic acid groups upon photoreduction of the secondary quinone (Q_B) in bacterial reaction centers from *Rhodobacter sphaeroides*: FTIR studies on the effects of replacing Glu H173. *Biochemistry* 37, 14457-14462 (1998)

54. Nabedryk, E., Breton, J., Hemalata, M. J., and Hanson, D. K. Fourier Transform Infrared Evidence of Proton Uptake by Glutamate L212 upon Reduction of the Secondary Quinone Q_B in the Photosyntehtic Reaction Center from *Rhodobacter capsulatus*. *Biochemistry* 39, 14654-14663 (2000)

55. Kleinfeld, D., Okamura, M. Y., and Feher, G. Electron transfer in reaction centers of *Rhodopseudomonas sphaeroides*: I. Determination of the charge recombination pathway of $D^+Q_AQ_B^-$ and free energy and kinetic relations between $Q_A^-Q_B$ and $Q_AQ_B^-$. *Biochim. Biophys. Acta* 766, 126-140 (1984)

56. Tandori, J., Baciou, L., Alexov, E., Maróti, P., Schiffer, M., Hanson, D. K., and Sebban, P. Revealing the involvement of extended hydrogen bond networks in the cooperative function between distant sites in bacterial reaction centers. *J. Biol. Chem.* 276, 45513-45515 (2001)

57. Tandori, J., Maróti, P., Alexov, E., Sebban, P., and Baciou, L. Key role of proline L209 in connecting the distant quinone pockets in the reaction center of *Rhodobacter sphaeroides. Proc. Natl. Acad. Sci. USA* 99, 6702-6706 (2002)

58. Maróti, P., Hanson, D. K., Schiffer, M., and Sebban, P. Long-range electrostatic interaction in the bacterial photosynthetic reaction centre. *Nature Struc. Biol.* 2, 1057-1059 (1995)

59. Miksovska, J., Kálman, L., Schiffer, M., Maróti, P., Sebban, P., and Hanson, D. K. In bacterial reaction centers rapid delivery of the second proton to Q_B can be achieved in the absence of L212Glu. *Biochemistry* 36, 12216-12226 (1997)

60. Alexov, E., Miksovska, J., Baciou, L., Schiffer, M., Hanson, D. K., Sebban, P., and Gunner, M. R. Modeling effects of mutations on the free energy of the first electron transfer from Q_A^- to Q_B in photosynthetic reaction centers. *Biochemistry* 39, 5940-5952 (2000)

61. Gunner, M. R., Saleh, M. A., Cross, E., ud-Doula, A., and Wise, M. Backbone dipoles generate positive potential

in all proteins: Origins and implications of the effect. *Biophys. J.* 78, 1126-1144 (2000)

62. Rabenstein, B., Ullmann, G. M., and Knapp, E.-W. Calculation of protonation patterns in proteins with structural relaxation and molecular ensembles - application to the photosynthetic reaction center. *Eur. Biophys. J.* 27, 626-637 (1998)

63. Rabenstein, B., Ullmann, G. M., and Knapp, E.-W. Electron Transfer between the Quinones in the Photosynthetic Reaction Center and Its Coupling to Conformational Changes. *Biochemistry* 39, 10487-10496 (2000)

64. Takahashi, E., and Wraight, C. A. Potentiation of Proton Transfer Function by Electrostatic Interactions in Photosynthetic Reaction Centers from *Rhodobacter sphaeroides*: First Results from Site Directed Mutation of the H-subunit. *Proc. Natl. Acad. Sci. USA* 93, 2640-2645 (1996)

65. Rongey, S. H., Paddock, M. L., Feher, G., and Okamura, M. Y. Pathway of Proton Transfer in Bacterial Reaction Centers: Second-site Mutation Asn-M44 –› Asp Restores Electron and Proton Transfer in Reaction Centers from the Photosynthetically Deficient Asp-L213 –› Asn Mutant of *Rhodobacter sphaeroides*. *Proc. Natl. Acad. Sci. USA* 90, 1325-1329 (1993)

66. Hanson, D. K., Baciou, L., Tiede, D. M., Nance, S. L., Schiffer, M., and Sebban, P. In bacterial reaction centers protons can diffuse to the secondary quinone by alternative pathways. *Biochim. Biophys. Acta* 1102, 260-265 (1992)

67. Okamura, M. Y., Paddock, M. L., McPherson, P. H., Rongey, S. H., and Feher, G. Proton transfer in bacterial reaction centers: Second site mutations Asn M44 to Asp and Arg M233 to Cys restore photosynthetic competence to Asp L213 to Asn mutants in RCs from *Rb. sphaeroides.* In: Research in Photosynthesis. Murata, N., Ed., Kluwer Academic Publishers, Dordrecht pp 349-356 (1992)

68. Paddock, M. L., Senft, M. E., Graige, M. S., Rongey, S. H., Turanchik, T., Feher, G., and Okamura, M. Y. Characterization of second site mutations show that fast proton transfer to Q_B^- is restored in bacterial reaction centers of *Rhodobacter sphaeroides* containing the Asp-L213 –› Asn lesion. *Photosynth. Res.* 55, 281-291 (1998)

69. Paddock, M. L., Axelrod, H. L., Abresch, E. C., Yeh, A. P., Rees, D. C., Feher, G., and Okamura, M. Y. Crystal structure of a photosynthetic revertant from *Rb. sphaeroides*: Mechanism of action of a long distant suppressor mutation. *Biophys. J.* 76, A141 (1999)

70. Nabedryk, E., Breton, J., Okamura, M. Y., and Paddock, M. L. Direct evidence of structural changes in reaction centers of *Rb. sphaeroides* containing suppressor mutations for Asp L213 –› Asn: A FTIR study of Q_B photoreduction. *Photosynth. Res.* 55, 293-299 (1998)

71. Rabenstein, B., Ullmann, G. M., and Knapp, E.-W. Energetics of Electron-Transfer and Protonation Reactions of the Quinones in the Photosynthetic Reaction Center of *Rhodopseudomonas viridis*. *Biochemistry* 37, 2488-2495 (1998)

72. Gunner, M. R., Nicholls, A., and Honig, B. Electrostatic potentials in *Rhopseudomonas viridis* reaction center: Implications for the driving force and directionality of electron transfer. *J. Phys. Chem.* 100, 4277-4291 (1996)

73. Breton, J., Nabedryk, E., Mioskowski, C., and Boullais, C. Protein-quinone interactions in photosynthetic bacterial reaction centers investigated by light-induced FTIR difference spectroscopy. In: The Reaction Center of Photosynthetic Bacteria: Structure and Dynamics. Michel-Beyerle, M.-E., Ed., Springer-Verlag, New York pp 381-394 (1996)

74. Breton, J., Nabedryk, E., Allen, J. P., and Williams, J. C. Electrostatic Influence of Q_A Reduction on the IR Vibrational Mode of the 10a-Ester C=O of H_A Demonstrated by Mutations at Residues Glu L104 and Trp L100 in Reaction Centers from *Rhodobacter sphaeroides*. *Biochemistry* 36, 4515-4525 (1997)

75. Zundel, G. Proton Polarizability of Hydrogen Bonds: Infrared Methods, Relevance to Electrochemical and Biological Systems. *Methods Enzymol.* 127, 439-455 (1986)

76. Zundel, G. Proton polarizability and proton transfer processes in hydrogen bonds and cation polarizabilities of other cation bonds. Their importance to understand processes in electrochemistry and biology. *Trends Phys. Chem.* 3, 129-156 (1992)

77. Breton, J., and Nabedryk, E. Proton uptake upon quinone reduction in bacterial reaction centers: IR signature and possible participation of a highly polarizable hydrogen bond network. *Photosynth. Res.* 55, 310-307 (1998)

78. LeCoutre, J., Tittor, J., Oesterhelt, D., and Gerwert, K. Experimental Evidence for Hydrogen-bonded Network Proton Transfer in Bacteriorhodopsin Shown by Fourier-transform Infrared Spectroscopy using Azide as Catalyst. *Proc. Natl. Acad. Sci. USA* 92, 4962-4966 (1995)

79. Rammelsberg, R., Huhn, G., Lübben, M., and Gerwert, K. Bacteriorhodopsin's intramolecular proton-release pathway consists of a hydrogen-bonded network. *Biochemistry* 37, 5001-5009. (1998)

80. McPherson, P. H., Schönfeld, M., Paddock, M. L., Okamura, M. Y., and Feher, G. Protonation and Free Energy Changes Associated with Formation of Q_BH_2 in Native and Glu-L212 –› Gln Mutant Reaction Centers from *Rhodobacter sphaeroides*. *Biochemistry* 33, 1181-1193 (1994)

81. Graige, M. S., Paddock, M. L., Feher, G., and Okamura, M. Y. Observation of the protonated semiquinone intermediate in isolated reaction centers from

Rhodobacter sphaeroides: Implications for the mechanism of electron and proton transfer in proteins. *Biochemistry* 38, 11465-11473 (1999)

82. Takahashi, E., and Wraight, C. A. Site-directed mutagenesis of Asp-H170 near the Q_B binding site of *Rhodobacter sphaeroides* reaction center. *Biophys. J.* 74, A76 (1998)

83. Verméglio, A. Secondary electron transfer in reaction centers of *Rhodopseudomonas sphaeroides*: Out-of-phase periodicity of two for the formation of ubisemiquinone and fully reduced ubiquinone. *Biochim. Biophys. Acta* 459, 516-524 (1977)

84. Verméglio, A., and Clayton, R. K. Kinetics of electron transfer between the primary and secondary electron acceptor in reaction centers from *Rhodopseudomonas sphaeroides*. *Biochim. Biophys. Acta* 461, 159-165 (1977)

85. Wraight, C. A. Electron acceptors of bacterial photosynthetic reaction centers II. H^+ binding coupled to secondary electron transfer in the quinone acceptor complex. *Biochim. Biophys. Acta* 548, 309-327 (1979)

86. Tiede, D. M., and Hanson, D. K. Protein Relaxation Following Quinone Reduction In Rhodobacter Capsulatus: Detection of Likely Protonation Linked Optical Absorbance Changes of the Chromophores. In: The Photosynthetic Reaction Center II. Breton, J., and Verméglio, A., Eds., Plenum Press, New York pp 341-350 (1992)

87. Tiede, D. M., Vazquez, J., Cordova, J., and Marone, P. A. Time-resolved electrochromism associated with the formation of quinone anions in the *Rhodobacter sphaeroides* R26 reaction center. *Biochemistry* 35, 10763-10775 (1996)

88. Maróti, P., and Wraight, C. A. Kinetic correlation between electron transfer and H^+-binding in reaction centers of photosynthetic bacteria *Rb. sphaeroides*. *Biophys. J.* 55, 182a (1989)

89. Takahashi, E., Maróti, P., and Wraight, C. A. Coupled proton and electron transfer pathways in the acceptor quinone complex of reaction centers from *Rhodobacter sphaeroides*. In: Electron and Proton Transfer in Chemistry and Biology. Diemann, E., Junge, W., Müller, A., and Ratazczak, H., Eds., Elsevier, Amsterdam pp 219-236 (1992)

90. Stowell, M. H. B., McPhillips, T. M., Rees, D. C., Soltis, S. M., Abresch, E., and Feher, G. Light-Induced Structural Changes in Photosynthetic Reaction Center: Implications for Mechanism of Electron-Proton Transfer. *Science* 276, 812-816 (1997)

91. Lancaster, C. R. D., and Michel, H. The coupling of light-induced electron transfer and proton uptake as derived from crystal structures of reaction centres from *Rhodopseudomonas viridis* modified at the binding site of the secondary quinone, Q_B. *Structure* 5, 1339-1359 (1997)

92. Graige, M. S., Feher, G., and Okamura, M. Y. Conformational gating of the electron transfer reaction $Q_A^- Q_B \rightarrow Q_A Q_B^-$ in bacterial reaction centers of *Rhodobacter sphaeroides* determined by a driving force assay. *Proc. Natl. Acad. Sci. USA* 95, 11679-11684 (1998)

93. Grafton, A. K., and Wheeler, R. A. Amino acid protonation states determine binding sites of the secondary ubiquinone and its anion in the *Rhodobacter sphaeroides* photosynthetic reaction center. *J. Phys. Chem. B* 103, 5380-5387 (1999)

94. Zachariae, U., and Lancaster, C. R. D. Proton uptake associated with the reduction of the primary quinone Q_A influences the binding site of the secondary quinone Q_B in *Rhodopseudomonas viridis* photosynthetic reaction centres. *Biochim. Biophys. Acta* 1505, 280-290 (2001)

95. Walden, S. E., and Wheeler, R. A. Protein conformational gate controlling binding site preference and migration for ubiquinone-B in the photosynthetic reaction center of*Rhodobacter sphaeroides*. *J. Phys. Chem. B* 106, 3001-3006 (2002)

96. Kuglstatter, A., Ermler, U., Michel, H., Baciou, L., and Fritzsch, G. X-ray structure analysis of photosynthetic reaction center variants from *Rhodobacter sphaeroides*: Structural changes induced by point mutations at position L209 modulate electron and proton transfer. *Biochemistry* 40, 4253-4260 (2001)

97. Tandori, J., Sebban, P., Michel, H., and Baciou, L. In *Rhodobacter sphaeroides* reaction centers, mutation of proline L209 to aromatic residues in the vicinity of a water channel alters the dynamic coupling between electron and proton transfer processes. *Biochemistry* 38, 13179-13187 (1999)

98. Breton, J., Boullais, C., Mioskowski, C., Sebban, P., Baciou, L., and Nabedryk, E. Vibrational spectroscopy favors a unique Q_B binding site at the proximal position in wild-type reaction centers and in the Pro-L209–›Tyr mutant from *Rhodobacter sphaeroides*. *Biochemistry* 41, 12921-12927 (2002)

99. Takahashi, E., Maróti, P., and Wraight, C. A. Site-directed mutagenesis of *Rhodobacter sphaeroides* reaction center: The role of Tyrosine L222. In: Current Research in Photosynthesis. Baltscheffsky, M., Ed., Kluwer Academic Publ., Dordrecht pp 169-172 (1990)

100. Shinkarev, V. P., and Wraight, C. A. The interaction of quinone and detergent with reaction centers of purple bacteria. I. Slow quinone exchange between reaction center micelles and pure detergent micelles. *Biophys. J.* 72, 2304-2319 (1997)

101. Ermler, U., Fritzsch, G., Buchanan, S. K., and Michel, H. Structure of the Photosynthetic Reaction Center from Rhodobacter sphaeroides at 2.65 Å Resolution: Cofactors and Protein-cofactor Interactions. *Curr. Biol. Structure* 2, 925-936 (1994)

102. Larson, J. W., and Wraight, C. A. Investigating the Role of Water in Reaction Center-Quinone Function by Osmotic Pressure. *Photosynth. Res.* 44, 65 (1995)

103. Li, J., Gilroy, D., Tiede, D. M., and Gunner, M. R. Kinetic phases in the electron transfer from $P^+Q_A^-Q_B$ to $P^+Q_AQ_B^-$ and the associated processes in *Rhodobacter sphaeroides* R-26 reaction centers. *Biochemistry* 37, 2818-2829 (1998)

104. Li, J., Takahashi, E., and Gunner, M. R. $-\Delta G_{AB}^o$ and pH dependence of the electron transfer from $P^+Q_A^-Q_B$ to $P^+Q_AQ_B^-$ in *Rhodobacter sphaeroides* reaction centers. *Biochemistry* 39, 7445-7454 (2000)

105. Ädelroth, P., Paddock, M. L., Tehrani, A., Beatty, J. T., Feher, G., and Okamura, M. Y. Identification of the Proton Pathway in Bacterial Reaction Centers: Decrease of Proton Transfer Rate by Mutation of surface Histidines at H126 and H128 and Chemical Rescue by Imidazole Identifies the Initial Proton Donors. *Biochemistry* 40, 14538-14546 (2001)

106. Wraight, C. A. Functional linkage between the Q_A and Q_B sites of photosynthetic reaction centers. In: Photosynthesis: Mechanisms and Effects. Garab, G., Ed., Kluwer Academic Publ., Dordrecht pp 693-698 (1998)

107. Prince, R. C., and Dutton, P. L. The primary acceptor of bacterial photosynthesis; its operating midpoint potential? *Arch. Biochem. Biophys.* 172, 329-334 (1976)

108. Prince, R. C., and Dutton, P. L. Protonation and the reducing potential of the primary electron acceptor. In: The Photosynthetic Bacteria. Clayton, R. K., and Sistrom, W. R., Eds., Plenum Press, New York pp 439-453 (1978)

109. Wraight, C. A. Oxidation-reduction physical chemistry of the acceptor quinone complex in bacterial photosynthetic reaction centers: Evidence for a new model of herbicide activity. *Israel J. Chem.* 21, 348-354 (1981)

110. Kálman, L., and Maróti, P. Stabilization of reduced primary quinone by proton uptake in reaction centers of *Rhodobacter sphaeroides*. *Biochemistry* 33, 9237-9244 (1994)

111. McComb, J. C., Stein, R. R., and Wraight, C. A. Investigations on the influence of headgroup substitution and isoprene side-chain length in the function of primary and secondary quinones of bacterial reaction centers. *Biochim. Biophys. Acta* 1015, 156-171 (1990)

112. Takahashi, E., Wells, T. A., and Wraight, C. A. Protein control of the redox potential of the primary acceptor quinone in reaction centers from *Rhodobacter sphaeroides*. *Biochemistry* 40, 1020-1028 (2001)

113. Mulkidjanian, A. Y. Conformationally controlled pK-switching in membrane proteins: One more mechanism specific to the enzyme catalysis? *FEBS Letters* 463, 199-204 (1999)

114. Baciou, L., and Michel, H. Interruption of the Water Chain in the Reaction Center from *Rhodobacter sphaeroides* Reduces the Rates of the Proton Uptake and of the Second Electron Transfer to Q_B. *Biochemistry* 34, 7967-7972 (1995)

115. Fritzsch, G., Ermler, U., and Michel, H. The water chains around Q_A and Q_B and other structural aspects of the reaction center from *Rb. sphaeroides*. In: Photosynthesis: From Light to Biosphere. Mathis, P., Ed., Kluwer Academic Publishers, Dordrecht pp 599-602. (1995)

116. Lavergne, J., Matthews, C., and Ginet, N. Electron and proton transfer on the acceptor side of the reaction center in chromatophores of *Rhodobacter capsulatus*: Evidence for direct protonation of the semiquinone state of Q_B. *Biochemistry* 38, 4542-4552 (1999)

117. Graige, M. S., Paddock, M. L., Bruce, J. M., Feher, G., and Okamura, M. Y. Mechanism of proton-coupled electron transfer for quinone (Q_B) reduction in reaction centers of *Rb. sphaeroides*. *J. Am. Chem. Soc.* 118, 9005-9016 (1996)

118. Stein, R. R. Inhibitor-quinone interactions in reaction centers from *Rhodopseudomonas sphaeroides*. In: Biophysics, University ofIllinois, Urbana-Champaign (1976)

119. Calvo, R., Abresch, E. C., Bittl, R., Feher, G., Hofbauer, W., Isaacson, R. A., Lubitz, W., Okamura, M. Y., and Paddock, M. L. EPR Study of the Molecular and Electronic Structure of the Semiquinone Biradical $Q_A^{\cdot-}$ $Q_B^{\cdot-}$ in Photosynthetic Reaction Centers from *Rb. sphaeroides*. *J. Am. Chem. Soc.* 122, 7327-7341 (2000)

120. Calvo, R., Isaacson, R., Paddock, M. L., Abresch, E. C., Okamura, M. Y., Maniero, A.-L., Brunel, L.-C., and Feher, G. EPR Study of the Semiquinone Biradical $Q_A^{\cdot-}$ $Q_B^{\cdot-}$ in Photosynthetic Reaction Centers from *Rb. sphaeroides* at 326 GHz: Determination of the Exchange Interaction J_0. *J. Phys. Chem. B* 105, 4053-4057 (2001)

121. Moser, C. C., Page, C. C., Chen, X., and Dutton, P. L. Effects of intervening medium on long-range biological electron transfer. *J. Biol. Inorg. Chem.*, 1-11 (1997)

122. Moser, C. C., Keske, J. M., Warncke, K., Farid, R. S., and Dutton, P. L. Nature of Biological Electron Transfer. *Nature* 355, 796-802 (1992)

123. Gray, H. B., and Winkler, J. R. Electron transfer in proteins. *Annu. Rev. Biochem.* 65, 537-561 (1996)

124. Gunner, M. R., and Dutton, P. L. Temperature and -ΔG dependence of the electron transfer from BPh^- to Q_A in reaction center protein from *Rhodobacter sphaeroides* with different quinones as Q_A. *J. Am. Chem. Soc.* 111, 3400-3412. (1989)

125. Allen, J. P., Williams, J. C., Graige, M., Paddock, M. L., Labahn, A., Feher, G., and Okamura, M. Y. Free energy

dependence of the direct charge recombination from the primary and secondary quinones in reaction centers from *Rhodobacter sphaeroides*. *Photosynth. Res.* 55, 227-233 (1998)

126. Labahn, A., Bruce, J. M., Okamura, M. Y., and Feher, G. Direct charge recombination from $D^+Q_AQ_B^-$ to DQ_AQ_B in bacterial reaction centers from *Rhodobacter sphaeroides* containing low potential quinone in the Q_A site. *Chem. Phys.* 97, 355-366 (1995)

127. Schmid, R., and Labahn, A. Temperature and free energy dependence of the direct charge recombination rate from the secondary quinone in bacterial reaction centers from *Rhodobacter sphaeroides*. *J. Phys. Chem. B* 104, 2928-2936 (2000)

128. Moser, C. C., Page, C. C., Farid, R., and Dutton, P. L. Biological Electron Transfer. *J. Bioenerg. Biomemb.* 27, 263-274 (1995)

129. Eigen, M. Proton Transfer, Acid-base Catalysis, and Enzymatic Hydrolysis. *Angew. Chem. Internat. Edit.* 3, 1-19 (1964)

130. Gutman, M., and Nachliel, E. The Dynamic Aspects of Proton Transfer Processes. *Biochim. Biophys. Acta* 1015, 391-414 (1990)

131. Dutton, P. L., Leigh, J. S., and Wraight, C. A. Direct measurement of the midpoint potential of the primary electron acceptor in *Rhodopseudomonas sphaeroides in situ* and in the isolated state: some relationships with pH and o-phenathroline. *FEBS Lett.* 36, 169-173 (1973)

132. McPherson, P. H., Nagarajan, V., Parson, W. W., Okamura, M. Y., and Feher, G. pH-dependence of the free energy gap between DQ_A and $D^+Q_A^-$ determined from delayed fluorescence in reaction centers from *Rhodobacter sphaeroides* R-26. *Biochim. Biophys. Acta* 1019, 91-94 (1990)

133. Gilson, M. K., Rashin, A., Fine, R., and Honig, B. On the calculation of electrostatic interactions in proteins. *J. Mol. Biol.* 183, 503-516 (1985)

134. Paddock, M. L., Feher, G., and Okamura, M. Y. Proton and electron transfer to the secondary quinone (Q_B) in bacterial centers: The effect of changing the electrostatics in the vicinity of Q_B by interchanging Asp and Glu at the L212 and L213 sites. *Biochemistry* 36, 14238-14249 (1997)

135. Maróti, P., Hanson, D. K., Baciou, L., Schiffer, M., and Sebban, P. Proton conduction within the reaction centers of *Rhodobacter capsulatus*: The electrostatic role of the protein. *Proc. Natl. Acac. Sci. U.S.A.* 91, 5617-5621 (1994)

136. Miksovska, J., Valerio-Lepiniec, M., Schiffer, M., Hanson, D. K., and Sebban, P. In bacterial reaction centers, a key residue suppresses mutational blockage of two different proton transfer steps. *Biochemistry* 37, 2077-2083 (1998)

137. Valerio-Lepiniec, M., Miksovska, J., Schiffer, M., Hanson, D. K., and Sebban, P. Mutations in the environment of the primary quinone facilitate proton delivery to the secondary quinone in bacterial photosynthetic reaction centers. *Biochemistry* 38, 390-398 (1999)

138. Morrison, L. E., Schelhorn, J. E., Cotton, T. E., Bering, C. L., and Loach, P. A. Electrochemical and Spectral Properties of Ubiquinone and Synthetic Analogs: Relevance to Bacterial Photosynthesis. In: Function of Quinones in Energy Conserving Systems. Trumpower, B. L., Ed., Academic Press, New York pp 35-58 (1982)

139. Shinkarev, V. P., Takahashi, E., and Wraight, C. A. Flash-induced Electric Potential Generation in Wild Type and L212EQ Mutant Chromatophores of *Rhodobacter sphaeroides*: Q_BH_2 is not Released from L212EQ Mutant Reaction Centers. *Biochim. Biophys. Acta* 1142, 214-216 (1993)

140. Abresch, E. C., Paddock, M. L., Stowell, M. H. B., McPhillips, T. M., Axelrod, H. L., Soltis, S. M., Rees, D. C., Okamura, M. Y., and Feher, G. Identification of proton transfer pathways in the X-ray crystal stucture of the bacterial reaction center from *Rhodobacter sphaeroides*. *Photosynth Res* 55, 119-125 (1998)

141. Utschig, L. M., Ohigashi, Y., Thurnauer, M. C., and Tiede, D. M. A new metal binding site in photosynthetic bacterial reaction centers that modulates Q_A to Q_B electron transfer. *Biochemistry* 37, 8278-8281 (1998)

142. Paddock, M. L., Graige, M. S., Feher, G., and Okamura, M. Y. Identification of the proton pathway in bacterial reaction centers: Inhibition of proton transfer by binding of Zn^{2+} or Cd^{2+}. *Proc Natl Acad Sci USA* 96, 6183-6188 (1999)

143. Axelrod, H. L., Abresch, E. C., Paddock, M. L., Feher, G., and Okamura, M. Y. Determination of the binding sites of the proton transfer inhibitors Cd^{2+} and Zn^{2+} in bacterial reaction centers. *Proc. Natl. Acad. Sci. USA* 97, 1542-1547 (2000)

144. Paddock, M. L., Feher, G., and Okamura, M. Y. Identification of the proton pathway in bacterial reaction centers: Replacement of Asp-M17 and Asp-L210 with Asn reduces the proton transfer rate in the presence of Cd^{2+}. *Proc. Natl. Acad. Sci. U.S.A.* 97, 1548-1553 (2000)

145. Paddock, M. L., Adelroth, P., Chang, C., Abresch, E. C., Feher, G., and Okamura, M. Y. Identification of the Proton Pathway in Bacterial Reaction Centers: Cooperation between Asp-M17 and Asp-L210 Facilitates Proton Transfer to the Secondary Quinone (Q_B). *Biochemistry* 40, 6893-6902 (2001)

146. Ädelroth, P., Paddock, M. L., Sagle, L. B., Feher, G., and Okamura, M. Y. Identification of the Proton Pathway

in Bacterial Reaction Centers: Both Protons Associated with Reduction of Q_B to Q_BH_2 Share a Common Entry Point. *Proc. Natl. Acad. Sci. U.S.A.* 97, 13086-13091 (2000)

147. Paddock, M. L., McPherson, P. H., Feher, G., and Okamura, M. Y. Pathway of proton transfer in bacterial reaction centers: Replacement of serine-L223 by alanine inhibits electron and proton transfers associated with reduction of quinone to dihydroquinone. *Proc. Natl. Acad. Sci. USA* 87, 6803-6807 (1990)

148. Michel, H., and Deisenhofer, J. Relevance of the photosynthetic reaction center from purple bacteria to the structure of photosyntem II. *Biochemistry* 27, 1-7 (1988)

149. Paddock, M. L., Feher, G., and Okamura, M. Y. Pathway of proton transfer in bacterial reaction centers: Futher investigations on the role of Ser-L223 studied by site-directed mutagenesis. *Biochemistry* 34, 15742-15750 (1995)

150. Dowd, P., and Zheng, Z. B. On the mechanism of the anticlotting action of vitamin E quinone. *Proc. Natl. Acad. Sci. USA* 92, 8171-8175 (1995)

151. Scheiner, S., and Hillenbrand, E. A. Modification of pK values caused by change in H-bond geometry. *Proc. Natl. Acad. Sci. USA* 82, 2741-2745 (1985)

152. Michel, H., Epp, O., and Deisenhofer, J. Pigment-protein interactions in the photosynthetic reaction center from *Rhodopseudomonas viridis*. *EMBO J.* 5, 2445-2451 (1986)

153. Deisenhofer, J., and Michel, H. The photosynthetic reaction center from the purple bacterium *Rhodopseudomonas viridis*. *Science* 245, 1463-1473 (1989)

154. Valerio-Lepiniec, M., Delcroix, J.-D., Schiffer, M., Hanson, D., and Sebban, P. A native electrostatic environment near Q_B is not sufficient to ensure rapid proton delivery in photosynthetic reaction centers. *FEBS Letters* 407, 159-163 (1997)

155. Hanson, D. K., Tiede, D. M., Nance, S. L., Chang, C.-H., and Schiffer, M. Site-specific and Compensatory Mutations Imply Unexpected Pathways for Proton Delivery to the Q_B Binding Site of the Photosynthetic Reaction Center. *Proc. Natl. Acad. Sci. USA* 90, 8929-8933 (1993)

156. Takahashi, E., and Wraight, C. A. Small Weak Acids Stimulate Proton Transfer Events in Site-Directed Mutants of the Two Ionizable Residues, Glu^{L212} and Asp^{L213}, in the Q_B-binding Site of *Rhodobacter sphaeroides* Reaction Centers. *FEBS* 283, 140-144 (1991)

157. Tittor, J., Soell, C., Oesterhelt, D., Butt, H. J., and Bamberg, E. A defective proton pump, point-mutated bacteriorhodopsin Asp96–›Asn, is fully reactivated by azide. *EMBO J.* 8, 3477-3482 (1989)

158. Link, T. A., Hagen, W. R., Pierik, A. J., Assmann, C., and von Jagow, G. *Eur. J. Biochem.* 208, 685-691 (1992)

159. Ullmann, G. M., Noodleman, L., and Case, D. A. Density functional calculation of pK_a values and redox potentials in the bovine Rieske iron-sulfur protein. *J. Biol Inorg. chem.* 7, 632-639 (2002)

160. McPherson, P. H., Okamura, M. Y., and Feher, G. Light-induced Proton Uptake by Photosynthetic Reaction Centers from *Rhodobacter sphaeroides* R-26.1. II. Protonation of the State $DQ_AQ_B^{2-}$. *Biochim. Biophys. Acta* 1144, 309-324 (1993)

161. Miksovska, J., Schiffer, M., Hanson, D. K., and Sebban, P. Proton uptake by bacterial reaction centers: The protein complex responds in a similar manner to the reduction of either quinone. *Proc. Natl. Acad. Sci. U.S.A.* 96, 14348-14353 (1999)

162. Lancaster, C. R. D., and Michel, H. Refined Crystal Structures of Reaction Centres from *Rhodopseudomonas viridis* in Complexes with the Herbicide Atrazine and Two Chiral Atrazine Derivatives also Lead to a New Model of the Bound Carotenoid. *J. Mol. Biol.* 286, 883-898 (1999)

163. Pines, E., Magnes, B.-Z., Lang, M. J., and Fleming, G. R. Direct measurement of intrinsic proton transfer rates in diffusion controlled reactions. *Chem. Phys. Lett.* 281, 413-420. (1997)

164. Brandsburg-Zabary, S., Fried, O., Marantz, Y., Nachliel, E., and Gutman, H. Biophysical aspects of intra-protein proton transfer. *Biochim. Biophys. Acta* 1458, 120-134. (2000)

165. Genosar, L., Cohen, B., and Huppert, D. Ultrafast direct photo-acid base reaction. *J. Phys. Chem. A* 104, 6689-6698. (2000)

166. Paddock, M. L., Ädelroth, P., Feher, G., Okamura, M. Y., and Beatty, J. T. Determination of Proton Transfer Rates by Chemical Rescue: Application to Bacterial Reaction Centers. *Biochemistry* 41, 14716-14725 (2002)

167. Gerencsér, L., and Maróti, P. Retardation of proton transfer caused by binding of the transition metal ion to bacterial reaction centers is due to pK_a shifts of key protonatable residues. *Biochemistry* 40, 1850-1860 (2001)

168. Eriksson, A. E., Jones, T. A., and Liljas, A. Refined structure of human carbonic anhydrase II at 2.0Å resolution. *PROTEINS: Structure, Function and Genetics* 4, 274-282 (1988)

169. Scolnick, L. R., and Christianson, D. W. X-ray crystallographic studies of alanine-65 variants of carbonic anhydrase II reveal the structural basis of compromised proton transfer in catalysis. *Biochemistry* 35, 16429-16434 (1996)

170. Tu, C., Qian, M., Earnhardt, J. N., Laipis, P. J., and Silverman, D. N. Properties of intramolecular proton transfer in carbonic anhydrase III. *Biophys. J.* 74, 3183-3189 (1998)

171. Silverman, D. N. Marcus rate theory applied to enzymatic proton transfer. *Biochim. Biophys. Acta* 1458, 88-103 (2000)

172. Toba, S., Colombo, G., and Merz, J., K. M. Solvent dynamics and mechanism of proton transfer in human carbonic anhydrase II. *J. Am. Chem. Soc.* 121, 2290-2302 (1999)

173. Lu, D., and Voth, G. A. Molecular Dynamics Simulations of Human Carbonic Anhydrase II: Insights into Experimental Results and the Role of Solvation. *Proteins* 33, 119-134 (1998)

174. Cui, Q., and Karplus, M. Is a "proton wire" concerted or stepwise? A model study of proton transfer in carbonic anhydrase. *J. Phys. Chem. B* 107, 1071-1078 (2003)

175. Greenleaf, W. B., and Silverman, D. N. Activation of the proton transfer pathway in catalysis by iron superoxide dismutase. *J. Biol. Chem.* 277, 49282-49286 (2002)

176. Luecke, H., Schobert, B., Richter, H. T., Cartailler, J. P., and Lanyi, J. K. Structural changes in bacteriorhodopsin during ion transport at 2 angstrom resolution. *Science* 286, 255-261 (1999)

177. Wikström, M. Water-gated mechanism of proton translocation by cytochrome c oxidase. *Biochim. Biophys. Acta* 1604, 61-65 (2003)

178. Silverman, D. N. Proton transfer in carbonic anhydrase measured by equilibrium isotope exchange. *Methods. Enzymol.* 249, 479-503 (1995)

179. Vuillemier, R., and Borgis, D. Molecular Dynamics of an Excess Proton in Water Using a Non-additive Valence Bond Force Field. *J. Mol. Struct.* 437, 555-565 (1998)

180. Marx, D., Tuckerman, M. E., Hutter, J., and Parrinello, M. The nature of the hydrated excess proton in water. *Nature* 397, 601-603 (1999)

181. Day, T. J. F., Schmitt, U. W., and Voth, G. A. The Mechanism of Hydrated Proton Transport in Water. *J. Am. Chem. Soc.* 122, 12027-12028 (2000)

182. Gopta, O. A., Cherapanov, D. A., Mulkidjanian, A. Y., Semenov, A. Y., and Bloch, D. A. Effect of temperature and surface potential on the electrogenic proton uptake in the Q_B site of the *Rhodobacter sphaeroides* photosynthetic reaction center: $Q_A^-Q_B^- \rightarrow Q_AQ_BH_2$ transition. *Photosynth. Res.* 55, 309-316 (1998)

183. Kleinfeld, D., Okamura, M. Y., and Feher, G. Electron-transfer kinetics in photosynthetic reaction centers cooled to cryogenic temperatures in the charge separated state: Evidence for light-induced structural changes. *Biochemistry* 23, 5780-5786 (1984)

184. Dean, J. A. Lange's handbook of chemistry., 13th ed., McGraw-Hill, New York (1985)

185. Weast, R. C. CRC handbook of chemistry and physics, 59th ed., CRC Press, West Palm Beach, FL (1978)

186. Christensen, J. J., Hansen, L. D., and Izatt, R. M. Handbook of Proton Ionization Heats and Related Thermodynamic Quantities, Wiley-Interscience, John Wiley & Sons, New York (1976)

187. Jackman, J. E., Merz, K. M., and Fierke, C. A. Disruption of the active site solvent network in carbonic anhydrase II decreases the efficiency of proton transfer. *Biochemistry* 35, 16421-16428 (1996)

188. Earnhardt, J. N., Qian, M., Tu, C., Laipis, P. J., and Silverman, D. N. Intramolecular proton transfer from multiple sites in catalysis by murine in carbonic anhydrase V. *Biochemistry* 37, 7649-7655 (1998)

189. Gutman, M., and Nachliel, E. The Dynamics of Proton Exchange Between Bulk and Surface Groups. *Biochim. Biophys. Acta* 1231, 123-138 (1995)

190. Gopta, O. A., Cherapanov, D. A., Junge, W., and Mulkidjanian, A. Y. Proton transfer from the bulk to the bound ubiquinone Q_B of the reaction center in chromatophores of *Rhodobacter sphaeroides*: Retarded conveyance by neutral water. *Proc. Natl. Acad. Sci. U.S.A.* 96, 13159-13164 (1999)

191. Teschke, O., Ceotto, G., and de Souza, E. F. Interfacial water dielectric-permittivity-profile measurements using atomic force microscopy. *Phys. Rev. E.* 64, 011605, 1-10 (2001)

192. Cherepanov, D. A., Feniouk, B. A., Junge, W., and Mulkidjanian, A. Y. Low dielectric permittivity of water at the membrane/water interface: Effect on the energy coupling mechanism of biological membranes. *Biophys. J.* 85, 1307-1316 (2003)

193. Gutman, M., and Nachliel, E. Time-resolved Dynamics of Proton Transfer in Proteinous Systems. *Annu. Rev. Phys. Chem.* 48, 329-356 (1997)

194. Sacks, V., Marantz, Y., Aagaard, A., Checover, S., Nachliel, E., and Gutman, M. The Dynamic Feature of the Proton Collecting Antenna of a Protein Surface. *Biochim. Biophys. Acta* 1365, 232-240 (1998)

195. Georgievskii, Y., Medvedev, E. S., and Stuchebrukhov, A. A. Proton transport via the membrane surface. *Biophys.J.* 82, 2833-2846. (2002)

196. Berg, H. C., and Purcell, E. M. Physics of chemoreception. *Biophys. J.* 20, 193-219 (1977)

197. Checover, S., Nachliel, E., Dencher, N. A., and Gutman, M. Mechanism of Proton Entry Into the Cytoplasmic Section of the Proton-conducting Channel of Bacteriorhodopsin. *Biochemistry* 36, 13919-13928 (1997)

198. Checover, S., Marantz, Y., Nachliel, E., and Gutman, M. Dynamics of the Proton Transfer Reaction on the Cytoplasmic Surface of Bacteriorhodopsin. *Biochemistry* 40, 4281-4292 (2001)

199. Marantz, Y., Nachliel, E., Aagaard, A., Brzezinski, P., and Gutman, M. The proton collecting function of the inner surface of cytochrome c oxidase from *Rhodobacter sphaeroides*. *Proc. Natl. Acad. Sci. USA* 95, 8590-8595 (1998)

200. Brown, L. S., Needleman, R., and Lanyi, J. K. Functional roles of aspartic acid residues at the cytoplasmic surface of bacteriorhodopsin. *Biochemistry* 38, 6855-6861 (1999)

201. Heberle, J., and Dencher, N. Surface-bound optical probes monitor proton translocation and surface potential changes during bacteriorhodopsin photocycle. *Proc. Natl. Acad. Sci. USA* 89, 5996-6000 (1992)

202. Heberle, J., Riesle, J., Thiedemann, G., Oesterhelt, D., and Dencher, N. Proton migration along the membrane surface and retarded surface to bulk transfer. *Nature* 370, 379-382 (1994)

203. Alexiev, U., Scherrer, P., Khorana, H. G., and Heyn, M. P. Rapid long-range proton diffusion along the surface of the purple membrane and delayed transfer into the bulk. *Proc. Natl. Acad. Sci. USA* 92, 372-376. (1995)

204. Tsukihara, T., Aoyama, H., Yamashita, E., Takashi, T., Yamaguichi, H., Shinzawa-Itoh, K., Nakashima, R., Yaono, R., and Yoshikawa, S. The Whole Structure of the 13-Subunit Oxidized Cytochrome c Oxidase at 2.8 Å. *Science* 272, 1136-1144 (1996)

205. Ostermeier, C., Iwata, S., and Michel, H. Cytochrome *c* Oxidase. *Current Opinion in Structural Biology* 6, 460-466 (1996)

206. Svensson-Ek, M., Abramson, J., Larsson, G., Tornroth, S., Brezezinski, P., and Iwata, S. The X-Ray Crystal Structures of Wild-Type and EQ(I-286) Mutant Cytochrome c Oxidases from *Rhodobacter sphaeroides*. *J.Mol.Biol* 321, 329-339 (2002)

207. Abramson, J., Riistama, S., Larsson, G., Jasaitis, A., Svensson-Ek, M., Laakkonen, L., Puustinen, A., Iwata, S., and Wikström, M. The structure of the heme-copper oxidase from *Escherichia coli* and its binding site for ubiquinone. *Nature Struc. Biol.* 7, 910-917 (2000)

208. Brzezinski, P., and Ädelroth, P. Pathways of Proton Transfer in Cytochrome *c* Oxidase. *J. Bioenerg. Biomemb.* 30, 99-107 (1998)

209. Getzoff, E. D., Cabelli, D. E., Fisher, C. L., Parge, H. E., Viezzoli, M. S., Banci, L., and Hallewell, R. A. Faster superoxide dismutase mutants designed by enhancing electrostatic guidance. *Nature* 358, 347-351 (1992)

210. Ripoll, D. R., Faerman, C. H., Axelsen, P. H., Silman, I., and Sussman, J. L. An electrostatic mechanism for substrate guidance down the aromatic gorge of acetylcholinesterase. *Proc Natl Acad Sci U S A.* 90, 5128-5132 (1993)

Footnotes

[1] The state PIQ_A^- is considered to be "closed" for productive photochemistry because $P^+I^-Q_A^-$ recombines so quickly (≤10 ns) that no trapping can occur by either electron donation to P^+ or transfer from I^-.

[2] The L and M subunit of all purple photosynthetic bacteria are highly homologous. Rba. sphaeroides and capsulatus are >75% identical and essentially 100% similar, but the M subunit in Rba. sphaeroides has 2 additional residues, inserted at about residue 38 and 106. Except where necessary, the amino acid numbering given here will refer to the Rba. sphaeroides sequence. The H subunits are much less similar, but, as yet, no H subunit mutational studies have been performed on any species other than Rba. sphaeroides.

[3] It should be noted that reversion to photosynthetic growth, which is the conventional selection procedure, is frequently a dubious criterion for functionally meaningful changes. Many of the second site revertants that have been further characterized exhibit electron transfer rates barely better than the primary (photosynthetically incompetent) mutants and some are still more than 3 orders of magnitude slower than the wild type.

[4] It may be mooted that the backbone potential "allows" the presence of the unusually large clusters of acidic groups in the quinone-binding region of the RC, especially the L and H-subunits, but the opposite logic may fit better: the acidic groups are required to overcome the positive potential, for general structural stability, but also specifically to restore reasonable and functional acidity to the semiquinone and quinol states.

[5] For calculation purposes, an intrinsic pK is defined as the value that would prevail if all other ionizable charges in a protein were neutralized, leaving only the partial charge set. Except for unusual (but often functionally important) cases, it is generally quite close to a solution pK.

[6] The kinetics observed in chromatophores (with native ubiquinone) are significantly faster than the main phases seen in isolated RCs, and are in line with the rate *vs*. $\Delta G°$ dependence reported by Li *et al* (104).

[7] 1 eV is frequently considered to be a suitable value for biological electron transfer reactions over a distance of 10 to 20 Å, in a "typical" protein environment (122, 123). For

the charge recombination reactions, $P^+Q_A^-$ —› PQ_A and $P^+Q_B^-$ —› PQ_B, the reorganization energy has been taken to be approx. 0.6-0.9 eV (122, 124, 125) and 1.1-1.4 eV (125-127), respectively. The smaller value for the former is considered to be consistent with the more apolar nature of the Q_A binding site, relative to that of Q_B. Since the inner reorganization contribution for P/P^+ is likely to be significantly smaller than for either quinone, one might expect the back reaction assays to underestimate the reorganization energy for Q_A to Q_B electron transfer. However, the greater distances and slower time scales for recombination will have an opposite effect on the outer reorganization energy.

Key Words: Photosynthetic Reaction Centers, Proton Transfer, Electrron Transfer, Quinones, *Rba. sphaeroides,* Review

Send all correspondence: Colin Wraight, Center for Biophysics & Computational Biology, MC–147, University of Illinois, 607 South Mathews Avenue, Urbana, IL 61801, U.S.A., Tel: 217-333-3245, Fax:217-244-6615, E-mail: cwraight@life.uiuc.edu